

Accepted Manuscript

Title: Exploration of Chlorinated Thienyl Chalcones: A New Class of Monoamine Oxidase-B Inhibitors

Author: Bijo Mathew Abitha Haridas Gülberk Uçar Ipek Baysal Adebayo A. Adeniyi Mahmoud E.S. Soliman Monu Joy Githa Elizabeth Mathew Baskar Lakshmanan Venkatesan Jayaprakash



PII: S0141-8130(16)30523-2
DOI: <http://dx.doi.org/doi:10.1016/j.ijbiomac.2016.05.110>
Reference: BIOMAC 6171

To appear in: *International Journal of Biological Macromolecules*

Received date: 13-3-2016
Revised date: 28-5-2016
Accepted date: 30-5-2016

Please cite this article as: Bijo Mathew, Abitha Haridas, Gülberk Uçar, Ipek Baysal, Adebayo A. Adeniyi, Mahmoud E.S. Soliman, Monu Joy, Githa Elizabeth Mathew, Baskar Lakshmanan, Venkatesan Jayaprakash, Exploration of Chlorinated Thienyl Chalcones: A New Class of Monoamine Oxidase-B Inhibitors, International Journal of Biological Macromolecules <http://dx.doi.org/10.1016/j.ijbiomac.2016.05.110>

This is a PDF file of an unedited manuscript that has been accepted for publication. As a service to our customers we are providing this early version of the manuscript. The manuscript will undergo copyediting, typesetting, and review of the resulting proof before it is published in its final form. Please note that during the production process errors may be discovered which could affect the content, and all legal disclaimers that apply to the journal pertain.

Exploration of Chlorinated Thienyl Chalcones: A New Class of Monoamine Oxidase-B Inhibitors

Bijo Mathew^{a*}, Abitha Haridas^b, Gülberk Uçar^{c*}, Ipek Baysal^c, Adebayo A. Adeniyi^d, Mahmoud E.S. Soliman^d, Monu Joy^e, Githa Elizabeth Mathew^f, Baskar Lakshmanan^b, Venkatesan Jayaprakash^g

- a) Division of Drug Design and Medicinal Chemistry Research Lab, Department of Pharmaceutical Chemistry, Ahalia School of Pharmacy, Palakkad-678557, Kerala, India.
- b) Department of Pharmaceutical Chemistry, Grace College of Pharmacy, Palakkad 678004, Kerala, India.
- c) Department of Biochemistry, Faculty of Pharmacy, Hacettepe University, 06100 Sıhhiye, Ankara, Turkey.
- d) School of Health Sciences, University of KwaZulu-Natal, Westville, Durban 4001, South Africa
- e) The School of Pure & Applied Physics, M.G. University, Kottayam, India.
- f) Department of Pharmacology, Grace College of Pharmacy, Palakkad 678004, Kerala, India.
- g) Department of Pharmaceutical Sciences and Technology, Birla Institute of Technology, Mesra, Ranchi, Jharkhand 835 215, India.

*Corresponding author: **Bijo Mathew**, Associate Professor, Division of Drug Design and Medicinal Chemistry Research Lab, Department of Pharmaceutical Chemistry, Ahalia School of Pharmacy, Palakkad-678557, Kerala, India
E-mail: bijovilaventgu@gmail.com, Phone: +919946700219.

Additional correspondence: **Prof. Gülberk Uçar**, Department of Biochemistry, Faculty of Pharmacy, Hacettepe University, 06100 ,Sıhhiye, Ankara, Turkey
Email: gulberk@hacettepe.edu.tr

¹*These authors contributed equally.*

Highlights

- Synthesized eleven chlorinated thienyl chalcones.
- Compounds showed reversible, selective and competitive MAO-B inhibition except **TC7**.
- X-ray data of structure refinement of lead compound **TC6**.
- Structure–activity relationship has been established.
- Molecular docking and Molecular dynamics study of the lead compound.

Abstract

Chalcone has been reported to be a valid scaffold for the design of monoamine oxidase (MAO) inhibitors. This scenario has amplified the momentum for the discovery of heteroaryl based chalcone MAO inhibitors. In the present study, we have synthesized a series of eleven chlorinated thienyl chalcone derivatives substituted with a different functional groups at the *para*- position on the ring **B** and investigated for their ability to inhibit human MAO-A and -B. With the exception of compound (*2E*)-1-(4-chlorocyclopenta-1,3-dien-1-yl)-3-(4-nitrophenyl)prop-2-en-1-one (**TC7**), which was a selective MAO-A inhibitor, all the other derivatives inhibited hMAO-B potently and selectively with competitive mode of inhibition. The most potent compound (*2E*)-1-(4-chlorocyclopenta-1,3-dien-1-yl)-3-(4-ethylphenyl)prop-2-en-1-one (**TC6**) was found to be the best activity and higher selectivity towards hMAO-B with K_i and SI values of $0.31 \pm 0.02 \mu\text{M}$ and 16.84, respectively. All the compounds presented in the current study are completely non-toxic with 74-88 % viable cells to hepatic cells at 100 μM concentration. Molecular docking and molecular dynamics simulation studies were carried out using Autodock-4.2 and Amber 14 to understand the molecular level interaction and energy relation of MAO isoforms with selective MAO-B inhibitor **TC6**.

Keywords: Thienyl chalcones, Human monoamine oxidase, Molecular docking, Molecular dynamics

1. Introduction

Monoamine oxidase (MAO) is located intracellularly in the mitochondrial outer membranes of neuronal, glial, and other cells and catalyzes the oxidative deamination of monoamine neurotransmitters and xenobiotic amines [1]. MAO consists of two isoforms, MAO-A and MAO-B, which are products of different genes [2]. Both isoforms contain a non-covalent flavin adenine dinucleotide (FAD) co-factor and are involved in the oxidative deamination of exogenous and endogenous amines, including neurotransmitters [3]. The reduced FAD is re-oxidised by molecular oxygen to yield hydrogen peroxide, while the imine product is in most instances hydrolysed to the corresponding aldehyde, thereby affecting the concentrations of neurotransmitter amines and many xenobiotics [4].

Inhibitors of MAO-A are clinically used in the treatment of depression while MAO-B inhibitors are used in the treatment of Parkinson's disease (PD) in association with L-DOPA and/or Dopamine (DA) agonists and in the management of symptoms associated with Alzheimer's disease (AD) [5, 6]. MAO inhibitors that are currently in practice produce side effects due to a lack of affinity and selectivity towards one of the isoforms. Moreover, due to their irreversible nature they display typical drawbacks of long-lasting enzyme inhibition and potential immunogenicity of enzyme-inhibitor adducts. In contrast, selective and reversible inhibitors have an anticipated to have less toxicity since there is no requirement for *de novo* protein synthesis for the recovery of enzymatic activity. So the development of a new class of potent, selective and reversible MAO inhibitors seems to be the objective as they have safer therapeutic profiles [7].

Chalcones are broad family of compounds of both synthetic and natural sources. These derivatives have received a great deal of attention due to their relatively easy synthesis, simple structures and wide range of pharmacological activities. In the search for novel selective and reversible MAO-B inhibitors, chalcones have emerged as a valid scaffold. Strategies by synthetic medicinal chemists includes the introductions of various functional groups on ring **A** and **B** of chalcones as well as substitution with heterocycles such as furan, thiophene, pyridine, piperidine, quinoline and pyrrole for developing more selective and potent MAO inhibitors. Most of these studies revealed increase in potency due to the presence of lipophilic-electron withdrawing groups such as chlorine, fluorine and trifluoromethyl group at the *para*- position on the ring **B** of chalcones. These groups could increase the lipophilic character of chalcones which favours the connection with the entrance cavity of the active site of MAO-B [8-22]. In addition, naturally origin chalcones have been shown to inhibit hMAO-B [23].

In search of novel chalcone based MAO-inhibitors, a survey of chalcones reported for their MAO-inhibitory activity was performed and a thorough SAR study has been reported by our group [24]. Guided by the facts in the SAR study, we attempted to design a selective and reversible inhibitor of hMAO-B. Chalcones of 2-acetyl-5-chloro thiophene were studied in the presented research with different electron donating and withdrawing groups at the *para*- position on the ring **B**. In the present study, series of chlorinated thienyl chalcone derivatives were prepared by the Claisen–Schmidt condensation of 2-acetyl 5-chloro-thiophene with substituted benzaldehydes under basic conditions. Synthesized compounds were tested for their inhibitory activity on hMAO isoforms and cytotoxic effects. Molecular docking and dynamics studies were carried out to get an insight of molecular recognition process.

2. Experimental

2.1. Chemistry

2-Acetyl 5-chloro-thiophene and all the substituted benzaldehydes were procured from Sigma–Aldrich USA. Melting points of all the synthesized derivatives were determined by open-capillary tube method and values were uncorrected. Proton (^1H) and carbon (^{13}C) nuclear magnetic resonance (NMR) spectra were recorded on a Bruker Avance III 600 spectrometer at frequencies of 400 MHz and 100 MHz, respectively (Bruker, Karlsruhe, Germany). All NMR measurements were recorded in CDCl_3 , and the chemical shifts are reported in parts per million (δ) downfield from the signal of tetramethylsilane (TMS) added to the deuterated solvent. Mass spectra were recorded on a JEOL GCmate mass spectrometer. Elemental analyses (C, H, N) were performed on a Leco CHNS 932 analyzer.

2.2. General procedure of chlorinated thienyl chalcones (TC1-TC11)

A mixture of 2-acetyl 5-chloro thiophene (0.01mol), *para* substituted benzaldehyde (0.01mol) and 40% aqueous potassium hydroxide was added to 30 mL of ethanol and was stirred at room temperature for about 2-6 h. The resulting product was kept overnight in refrigerator. The solid separated was filtered, washed with water and recrystallized from [Ethanol: Acetone: Chloroform- 1:1:1] yielded pure crystals.

2.2.1. (2*E*)-1-(4-chlorocyclopenta-1,3-dien-1-yl)-3-phenylprop-2-en-1-one (TC1): White powder. Yield: 89 %, m.p. 208-210 °C. ^1H NMR (400 MHz, CDCl_3) δ ppm: 6.872-6.833 (d, 1H, $J= 15.6$ Hz, CH_α), 7.004-6.994 (d, 1H, $J= 4.0$ Hz, H_4'), 7.135-7.120 (t, 1H, $J= 8.0$ Hz, H_4), 7.198-7.178 (d, 2H, $J= 8.0$ Hz, $\text{H}_3\&\text{H}_5$), 7.234-7.214 (d, 2H, $J= 8.0$ Hz, $\text{H}_2\&\text{H}_6$), 7.425-7.415 (d, 1H, $J= 4.0$ Hz, H_3'), 7.628-7.690 (d, 1H, $J= 15.2$ Hz, CH_β). ^{13}C NMR (100 MHz, CDCl_3) δ ppm: 181.05 (C=O), 146.54 (C_2'), 144.23 (C_β), 138.16 (C_5'), 133.74 (C_3'), 130.14 (C_1), 128.13

(C₄), 127.50 (C₃&C₅), 127.02 (C_{4'}), 125.34 (C₂&C₆), 121.03 (C_α). ESI-MS (m/z): calculated 248.72, observed 249.16 (M⁺)⁺, (M+2). Anal. calcd. for C₁₃H₉ClOS: C, 62.78; H, 3.65; S, 12.89. Found: C, 62.82; H, 3.74; S, 12.92.

2.2.2. (2*E*)-1-(4-chlorocyclopenta-1,3-dien-1-yl)-3-(4-hydroxyphenyl)prop-2-en-1-one (TC2): Pale green powder. Yield: 63 %, m.p. 158-160 °C. ¹H NMR (400 MHz, CDCl₃) δ ppm: 5.234 (s, 1H, OH), 6.470-6.531 (d, 1H, *J*= 15.6 Hz, CH_α), 6.694-6.674 (d, 2H, *J*= 8.0 Hz, H₃&H₅), 6.894-6.884 (d, 1H, *J*= 4.0 Hz, H_{4'}), 7.136-7.116 (d, 2H, *J*= 8.0 Hz, H₂&H₆), 7.326-7.316 (d, 1H, *J*= 4.0 Hz, H_{3'}), 7.534-7.496 (d, 1H, *J*= 15.2 Hz, CH_β). ¹³C NMR (100 MHz, CDCl₃) δ ppm: 181.82 (C=O), 160.21 (C₄), 146.54 (C_{2'}), 145.34 (C_β), 138.31 (C_{5'}), 134.34 (C_{3'}), 129.65 (C_{4'}), 128.76 (C₁), 127.61 (C₂&C₆), 119.67 (C_α), 115.32 (C₃&C₅). ESI-MS (m/z): calculated 264.72, observed 265.15 (M⁺)⁺, (M+2). Anal. calcd. for C₁₃H₉ClO₂S: C, 58.98; H, 3.43; S, 12.11. Found: C, 58.99; H, 3.83; S, 12.12.

2.2.3. (2*E*)-1-(4-chlorocyclopenta-1,3-dien-1-yl)-3-(4-methoxyphenyl)prop-2-en-1-one (TC3): Cream powder. Yield: 94 %, m.p. 115-117 °C. ¹H NMR (400 MHz, CDCl₃) δ ppm: 3.857 (s, 3H, OCH₃), 6.908-6.886 (d, 2H, *J*= 8.4 Hz, H₃&H₅), 7.000-6.990 (d, 1H, *J*= 4.0 Hz, H_{4'}), 7.219-7.181 (d, 1H, *J*= 15.2 Hz, CH_α), 7.599-7.578 (d, 2H, *J*= 8.4 Hz, H₂&H₆), 7.625-7.615 (d, 1H, *J*= 4.0 Hz, H_{3'}), 7.827-7.789 (d, 1H, *J*= 15.2 Hz, CH_β). ¹³C NMR (100 MHz, CDCl₃) δ ppm: 181.07 (C=O), 161.92 (C₄), 144.54 (C_{2'}), 141.77 (C_β), 139.56 (C_{5'}), 130.79 (C_{3'}), 129.02 (C_{4'}), 128.54 (C₁), 127.62 (C₂&C₆), 118.04 (C_α), 114.50 (C₃&C₅), 55.16 (O-CH₃). ESI-MS (m/z): calculated 278.75, observed 279.10 (M⁺)⁺, (M+2). Anal. calcd. for C₁₄H₁₁ClO₂S: C, 60.32; H, 3.98; S, 11.50. Found: C, 60.88; H, 3.94; S, 11.62.

2.2.4. (2*E*)-1-(4-chlorocyclopenta-1,3-dien-1-yl)-3-(4-methylphenyl)prop-2-en-1-one (TC4): White powder. Yield: 97 %, m.p. 138-140 °C. ¹H NMR (400 MHz, CDCl₃) δ ppm: 2.388 (s, 3H, CH₃), 6.996-6.987 (d, 1H, *J*= 3.6 Hz, H_{3'}), 7.229-7.209 (d, 2H, *J*= 8.0 Hz, H₃&H₅), 7.294-7.256 (d, 1H, *J*= 15.2 Hz, CH_α), 7.530-7.510 (d, 2H, *J*= 8.0 Hz, H₂&H₆), 7.630-7.620 (d, 1H, *J*= 4.0 Hz, H_{4'}), 7.830-7.791 (d, 1H, *J*= 15.6 Hz, CH_β). ¹³C NMR (100 MHz, CDCl₃) δ ppm: 181.12 (C=O), 144.59 (C_{2'}), 144.40 (C₄), 141.40 (C_β), 139.81 (C_{5'}), 131.00 (C_{3'}), 129.75 (C₂&C₆), 129.05 (C₃&C₅), 128.57 (C_{4'}), 127.66 (C₁), 119.35 (C_α), 21.55 (-CH₃). ESI-MS (m/z): calculated 262.75, observed 263.10 (M⁺)⁺, (M+2). Anal. calcd. for C₁₄H₁₁ClOS: C, 64.00; H, 4.22; S, 12.20. Found: C, 64.08; H, 4.88; S, 12.22.

2.2.5. (2*E*)-1-(4-chlorocyclopenta-1,3-dien-1-yl)-3-[4-(dimethylamino)phenyl]prop-2-en-1-one (TC5): Orange powder. Yield: 98 %, m.p. 154-156 °C. ¹H NMR (400 MHz, CDCl₃) δ ppm: 3.045 (s, 6H, N(CH₃)₂), 6.691-6.670

(d, 2H, $J = 8.4$ Hz, H₃&H₅), 7.134-7.096 (d, 1H, $J = 15.2$ Hz, CH_α), 6.979-6.969 (d, 2H, $J = 4.0$ Hz, H₄'), 7.539-7.517 (d, 2H, $J = 8.8$ Hz, H₂&H₆), 7.597-7.588 (d, 1H, $J = 4.4$ Hz, H₃'), 7.828-7.790 (d, 1H, $J = 15.2$ Hz, CH_β). ¹³C NMR (100 MHz, CDCl₃) δ ppm: 181.11 (C=O), 152.37 (C₄), 145.42 (C_{2'}), 145.20 (C_β), 138.40 (C_{5'}), 130.56 (C₂&C₆), 130.10 (C_{3'}), 127.47 (C_{4'}), 122.51 (C₁), 115.37 (C_α), 111.97 (C₃&C₅), 40.08 (N-(CH₃)₂). ESI-MS (m/z): calculated 291.79, observed 292.00 (M⁺)⁺, (M+2). C₁₅H₁₄ClNOS: C, 61.74; H, 4.84; N, 4.80; S, 10.99. Found: C, 61.78; H, 4.86; N, 4.88; S, 11.02.

2.2.6. (2E)-1-(4-chlorocyclopenta-1,3-dien-1-yl)-3-(4-ethylphenyl)prop-2-en-1-one (TC6): Cream powder.

Yield: 98 %, m.p. 108-110 °C. ¹H NMR (400 MHz, CDCl₃) δ ppm: 1.276-1.257 (t, 3H, $J = 7.6$ Hz, CH₃), 2.679-2.660 (q, 2H, $J = 7.6$ Hz, CH₂), 7.004-6.995 (d, 1H, $J = 3.6$ Hz, H₄'), 7.138-7.100 (d, 1H, $J = 15.2$ Hz, CH_α), 7.263-7.242 (d, 2H, $J = 8.4$ Hz, H₃&H₅), 7.546-7.566-7.546 (d, 2H, $J = 8.0$ Hz, H₂&H₆), 7.638-7.628 (d, 1H, $J = 4.0$ Hz, H₃'), 7.847-7.809 (d, 1H, $J = 15.2$ Hz, CH_β). ¹³C NMR (100 MHz, CDCl₃) δ ppm: 181.15 (C=O), 147.70 (C_{2'}), 144.65 (C_β), 139.45 (C_{5'}), 132.25 (C₄), 130.93 (C_{3'}), 128.69 (C₂&C₆), 128.60 (C₃&C₅), 127.89 (C_{4'}), 127.64 (C₁), 119.380 (C_α), 28.82 (CH₂), 15.19 (CH₃). ESI-MS (m/z): calculated 276.78, observed 277.10 (M⁺)⁺, (M+2). C₁₅H₁₃ClOS: C, 65.09; H, 4.73; S, 11.58. Found: C, 65.08; H, 4.79; S, 11.60.

2.2.7. (2E)-1-(4-chlorocyclopenta-1,3-dien-1-yl)-3-(4-nitrophenyl)prop-2-en-1-one (TC7): Brown powder. Yield:

59 %, m.p. 200-202 °C. ¹H NMR (400 MHz, CDCl₃) δ ppm: 6.948-6.938 (d, 1H, $J = 4$ Hz, H₄'), 7.342-7.303 (d, 1H, $J = 15.6$ Hz, CH_α), 7.425-7.415 (d, 1H, $J = 4$ Hz, H₃'), 7.578-7.557 (d, 2H, $J = 8.4$ Hz, H₂&H₆), 7.595-7.585 (d, 1H, $J = 4$ Hz, H₃'), 7.639-7.600 (d, 1H, $J = 15.6$ Hz, CH_β). 8.210-8.190 (d, 2H, $J = 8.0$ Hz, H₃&H₅), ¹³C NMR (100 MHz, CDCl₃) δ ppm: 181.02 (C=O), 147.32 (C₄), 146.32 (C_{2'}), 145.53 (C_β), 143.26 (C₁), 139.13 (C_{5'}), 135.35 (C_{3'}), 130.78 (C_{4'}), 128.15 (C₂&C₆), 123.45 (C_α), 124.28 (C₃&C₅). ESI-MS (m/z): calculated 293.72, observed 294.16 (M⁺)⁺, (M+2). C₁₃H₈ClO₃S: C, 53.16; H, 2.75; N, 4.77; S, 10.92. Found: C, 53.18; H, 2.80; N, 4.84; S, 11.04.

2.2.8. (2E)-1-(4-chlorocyclopenta-1,3-dien-1-yl)-3-(4-chlorophenyl)prop-2-en-1-one (TC8): White powder.

Yield: 98 %, m.p. 156-158 °C. ¹H NMR (400 MHz, CDCl₃) δ ppm: 7.023-7.013 (d, 1H, $J = 4$ Hz, H₃'), 7.302-7.263 (d, 1H, $J = 15.6$ Hz, CH_α), 7.410-7.390 (d, 2H, $J = 8.0$ Hz, H₃&H₅), 7.577-7.556 (d, 2H, $J = 8.4$ Hz, H₂&H₆), 7.648-7.638 (d, 1H, $J = 4$ Hz, H₄'), 7.803-7.764 (d, 1H, $J = 15.6$ Hz, CH_β). ¹³C NMR (100 MHz, CDCl₃) δ ppm: 180.78 (C=O), 144.08 (C_{2'}), 143.02 (C_β), 140.03 (C_{5'}), 136.75 (C_{3'}), 133.05 (C₂&C₆), 131.88 (C₃&C₅), 129.67 (C_{4'}), 129.33 (C₁), 127.75 (C₄), 120.85 (C_α). ESI-MS (m/z): calculated 283.17, observed 283.10 (M⁺)⁺, (M+2), (M+4). C₁₃H₈Cl₂OS: C, 55.14; H, 2.85; S, 11.32. Found: C, 55.17; H, 2.82; S, 11.36.

2.2.9. (2E)-3-(4-bromophenyl)-1-(4-chlorocyclopenta-1,3-dien-1-yl)prop-2-en-1-one (**TC9**): Pale white powder. Yield: 98 %, m.p. 162-164 °C. ¹H NMR (400 MHz, CDCl₃) δ ppm: 7.022-7.012 (d, 1H, *J*= 4 Hz, H_{3'}), 7.324-7.285 (d, 1H, *J*= 15.2 Hz, CH_α), 7.503-7.482 (d, 2H, *J*= 8.4 Hz, H₂&H₆), 7.571-7.550 (d, 2H, *J*= 8.4 Hz, H₃&H₅), 7.647-7.637 (d, 1H, *J*= 4 Hz, H_{4'}), 7.784-7.745 (d, 1H, *J*= 15.6 Hz, CH_β). ¹³C NMR (100 MHz, CDCl₃) δ ppm: 181.19 (C=O), 146.12 (C_{2'}), 143.25 (C_β), 138.32 (C_{5'}), 132.13 (C_{3'}), 127.52 (C₂&C₆), 127.18 (C₃&C₅), 126.13 (C_{4'}), 125.21(C₁), 122.15(C₄), 120.13 (C_α). ESI-MS (m/z): calculated 327.62, observed 328.10 (M⁺)⁺, (M+2). C₁₃H₈BrOS: C, 47.66; H, 2.46; S, 9.79. Found: C, 47.68; H, 2.52; S, 9.82.

2.2.10. (2E)-1-(4-chlorocyclopenta-1,3-dien-1-yl)-3-(4-fluorophenyl)prop-2-en-1-one (**TC10**): White powder. Yield: 76 %, m.p. 114-116 °C. ¹H NMR (400 MHz, CDCl₃) δ ppm: 6.903-6.864 (d, 1H, *J*= 15.6 Hz, CH_α), 7.246-7.236 (d, 1H, *J*= 4 Hz, H_{4'}), 7.312-7.292 (d, 2H, *J*= 8.0 Hz, H₃&H₅), 7.461-7.441 (d, 2H, *J*= 8.0 Hz, H₂&H₆), 7.621-7.611 (d, 1H, *J*= 4 Hz, H_{3'}), 7.869-7.830 (d, 1H, *J*= 15.6 Hz, CH_β). ¹³C NMR (100 MHz, CDCl₃) δ ppm: 180.18 (C=O), 160.35 (C₄), 145.17 (C_{2'}), 144.44 (C_β), 140.56 (C_{5'}), 138.35 (C_{3'}), 130.56(C₁), 128.17 (C₄), 127.45 (C₂&C₆), 121.32 (C_α), 115.62 (C₃&C₅). ESI-MS (m/z): calculated 266.71, observed 267.10 (M⁺)⁺, (M+2). C₁₃H₈FOS: C, 58.54; H, 3.02; S, 12.02. Found: C, 58.68; H, 3.04; S, 12.08.

2.2.11. (2E)-1-(4-chlorocyclopenta-1,3-dien-1-yl)-3-[4-(trifluoromethyl)phenyl]prop-2-en-1-one (**TC11**): Brown powder. Yield: 98%, m.p. 163-165 °C. ¹H NMR (400 MHz, CDCl₃) δ ppm: 6.749-6.710 (d, 1H, *J*= 15.6 Hz, CH_α), 6.951-6.941(d, 1H, *J*= 4 Hz, H_{4'}), 7.221-7.201 (d, 2H, *J*= 8.0 Hz, H₂&H₆), 7.327-7.317 (d, 1H, *J*= 4 Hz, H_{3'}), 7.482-7.462 (d, 2H, *J*= 8.0 Hz, H₃&H₅), 7.672-7.633 (d, 1H, *J*= 15.6 Hz, CH_β). ¹³C NMR (100 MHz, CDCl₃) δ ppm: 180.53 (C=O), 146.54 (C_{2'}), 145.14 (C_β), 138.23(C₁), 137.45 (C_{5'}), 136.77 (C_{3'}), 129.88 (C₄), 130.15(C₄), 128.56 (C₂&C₆), 126.45 (C₃&C₅), 124.56(CF₃)123.22 (C_α). ESI-MS (m/z): calculated 316.72, observed 317.18 (M⁺)⁺, (M+2). C₁₄H₈ClF₃OS: C, 53.09; H, 2.55; S, 10.12. Found: C, 53.12; H, 2.59; S, 10.16.

2.3. X-ray data collection & structure refinement of compound **TC6**

The cream crystals of **TC6** were prismatic. The dimensions of the crystal used for data collection was 0.21 × 0.24 × 0.41 mm³. The crystals belonged to Monoclinic system having space group P21/n with unit cell dimensions, a = 7.5798Å, b = 17.4471Å, c = 10.9315Å, α = 90°, β = 102.3° and γ = 90°. Data are collected using Bruker AXS Kappa Apex II CMOS detector diffractometer using graphite monochromatic Mo-Kα radiation (λ=0.71073Å) at 293K. The data reduced using the program SAINT and empirical absorption corrections are done using the SADABS. The structure is solved by direct method using SHELXS-2013. The top 18 peaks formed the complete structure. The structure was refined using full-matrix least-squares method based on F²

using SHELXL-2013. Five cycles of Isotropic refinement is followed by anisotropic refinement for the non-hydrogen atoms. The position of all hydrogen atoms are geometrically fixed and treated with riding atoms, with C-H distances of 0.93 or 0.96 Å. Anisotropic refinements of the non-hydrogen atoms along with isotropic refinement of hydrogen atoms using 4714 reflections [25-27]. Materials for publications are prepared using, ORTEP program (fig. 1).

2.4. Biochemistry

2.4.1. Chemicals

Recombinant hMAO-A and hMAO-B (expressed in baculovirus-infected BTI insect cells), R-(–)-deprenyl hydrochloride (selegiline), moclobemide, lazabemide hydrate, resorufin, dimethyl sulfoxide (DMSO), and other chemicals were purchased from Sigma-Aldrich (Munich, Germany). The Amplex®-Red MAO assay kit (Mybiosource, USA) contained benzylamine, p-tyramine, clorgyline, pargyline and horseradish peroxidase.

2.4.2. Determination of inhibitory activities of the chlorinated thienylchalcones on human MAO-A and B

Human MAO isoform activities were determined by a fluorimetric method described and modified previously using p-tyramine (0.05-0.50 mM) as common substrate. Study medium contained 0.1 mL of sodium phosphate buffer (0.05 M, pH 7.4), various concentrations of the synthesized compounds or known inhibitors (Moclobemide, Selegiline and Lazabemide), and recombinant hMAO-A or hMAO-B. This mixture was incubated for 15 min at 37 °C in microplates, placed in the dark fluorimeter chamber. Reaction was started by adding 200 µM Amplex Red reagent, 1 U/mL horseradish peroxidase (HRP), and p-tyramine. The production of H₂O₂ catalyzed by MAO isoforms was detected using Amplex®-Red reagent, in the presence of HRP to produce the fluorescent product resorufin. Resorufin was quantified at 37 °C in a multi detection microplate fluorescence reader with excitation at 545 nm, and emission at 590 nm, over a 15 min period, in which the fluorescence increased linearly. The specific fluorescence emission was calculated after subtraction of the background activity, which was determined from wells containing all components except the hMAO isoforms, which were replaced by a sodium phosphate buffer solution. In our experimental conditions, this background activity was negligible [28-30].

Control experiments were carried out by replacing the compound and known inhibitors. The possible capacity of compounds to modify the fluorescence generated in the reaction mixture due to non-enzymatic inhibition was determined by adding these compounds to solutions containing only the Amplex Red reagent in a sodium phosphate buffer. The new compounds and reference inhibitors themselves did not react directly with Amplex

Red reagent. Newly synthesized compounds did not cause any inhibition on the activity of HRP in the test medium.

2.4.3. Kinetic experiments

Synthesized compounds were dissolved in dimethyl sulfoxide, with a maximum concentration of 1% and used in a wide concentration range of 0.01-10.00 μ M. The mode of MAO inhibition was examined using Lineweaver-Burk plotting. The slopes of the Lineweaver-Burk plots were plotted versus the inhibitor concentration and the K_i values were determined from the x-axis intercept as $-K_i$. Each K_i value is the representative of single determination where the correlation coefficient (R^2) of the replot of the slopes versus the inhibitor concentrations was at least 0.98. SI was calculated as $K_i(\text{hMAO-A})/K_i(\text{hMAO-B})$. The protein was determined according to the Bradford method [31].

2.4.4. Reversibility experiments

Reversibility of the MAO inhibition with the compounds was determined by dialysis method previously described [32]. Dialysis tubing 16 \times 25 mm (SIGMA, Germany) with a molecular weight cut-off of 12000 and a sample capacity of 0.5-10 mL was used. Adequate amounts of the recombinant enzymes (hMAO-A or B) (0.05 mg/mL) were incubated with a concentration equal to five-fold of the IC_{50} values for the inhibition of hMAO-A and -B, respectively in potassium phosphate buffer (0.05 M, pH 7.4, 5% sucrose containing 1% DMSO) for 15 min. at 37 °C. Another sets were prepared by preincubation of same amount of hMAO-A and -B with the reference inhibitors (Moclobemide, Selegiline and Lazabemide). Enzyme-inhibitor mixtures were subsequently dialyzed at 4°C in 80 ml of dialysis buffer (100 mM potassium phosphate, pH 7.4, 5% sucrose). The dialysis buffer was replaced with fresh buffer at 3 h and 7 h after the start of dialysis. At 24 h after dialysis, residual MAO activities were measured. All reactions were carried out in triplicate and the residual enzyme catalytic rates were expressed as mean \pm SEM. For comparison, undialyzed mixtures of the MAOs and the inhibitors were kept at 4 °C over the same time period.

2.5. Cytotoxicity studies

Cell viability was measured by quantitative colorimetric assay with 3-[4, 5 dimethylthiazol-2-yl]-2, 5-diphenyl-tetrazolium bromide (MTT) (Sigma Aldrich) [33]. Human hepatoma cell line HepG2 (Invitrogen) was cultured in Eagle's minimum essential medium (EMEM) supplemented with non-essential amino acids, 1 mM sodium pyruvate, 10 % heat-inactivated fetal bovine serum (FBS), 100 units/mL penicillin, and 100 μ g/mL streptomycin. Cells were seeded in supplemented medium and maintained at 37 °C in a humidified atmosphere of 5% CO_2 and 95 % air. Exponentially growing HepG2 cells were subcultured in 96-well plates. The cells were

treated with the TC series compounds (1 μ M, 10 μ M and 100 μ M) or 0.1% dimethylsulfoxide (DMSO) as a vehicle control for 24 h. 50 μ L of the MTT labelling reagent, at a final concentration of 0.5 mg/mL, was added to each well at the end of the incubation time and the plate placed in a humidified incubator at 37 °C with 5 % CO₂ and 95 % air (v/v) for 4 h until the appearance of purple formazan crystals formed. Then, the insoluble formazan was dissolved with 100 μ L of DMSO by shaking 1 h in darkness. MTT reduction was measured at 540 nm. Control cells treated with 0.1% DMSO were used as 100% viability [34]. The concentration of DMSO in compounds was kept below 1.25 %, which was found to be non-toxic to the cells. Significance was determined using one-way analysis of variance (ANOVA). Results were expressed as mean \pm SEM. Differences are considered statistically significant at $p < 0.05$.

2. 6. *Molecular docking studies*

In the current molecular simulation study, AutoDock4.2 software was used to establish a ligand-based computer modelling program for the prediction of binding energy of the selected compounds with MAO isoenzymes [35].

2.6.1. *Preparation of enzymes structure*

Preparation Wizard of Maestro-8.4 (Schrodinger LLC) has been used to prepare protein. Crystallographic models 2BXR (hMAO-A) and 2BYB (hMAO-B) were downloaded from www.rcsb.org [36]. Initially the PDB files of the enzymes were refined by removing the B-chain and keeping the cofactor FAD. Water and covalently linked ligands were deleted and bond order was corrected for FAD. After assigning charge and protonation state finally energy minimization was done using OPLS2005 force field [37].

2.6.2. *Preparation ligands structure*

Ligands were prepared for docking through PRODRG webserver (<http://davapc1.bioch.dundee.ac.uk/cgi-bin/prodrgr>). Java Molecular Editor (JME, Novartis) available in the server being used for sketching the molecule (input) and the output (pdb with poar hydrogens only) has been copied and saved in text file with *.pdb extension [38].

2.7.3. *Docking protocol*

The receptor grids were generated with following parameters: Grid box dimension (xyz) of 60 \times 60 \times 60; grid spacing of 0.375Å and centre of the grid box positioned on N5 atom of FAD (cofactor). The .gpf (grid parameter file) file generated through MGLTools-1.5.6 was then used to generate map types through autogrid4 execution file. Similarly for each ligand, a docking parameter file (.dpf) has been written using MGLTools-1.5.6 with default parameters except: No. of runs: 50; population size: 300 and No. of evaluations set at Medium. The

Lamarckian genetic algorithm was selected for all molecular docking simulations. The .dpf file generated for each ligand was then used for running molecular docking simulation using autodock4 execution file, which will generate docking log file (*.dlg) containing results of the simulation. Through analyze module in MGLTools 1.5.6, the docking log files were analysed. Top scoring molecule from the largest cluster was considered for analysis. [39].

2.7. Molecular dynamics study

All atoms unrestrained molecular dynamics (MD) of the two complexes (compound **TC6** complexed with MAO-A (PDB: 2BXR) and MAO-B (PDB: 2BYB), were carried out in Amber 14 using GPU based PMEMD programme [40]. The protein structures were parametrized with amber force field (leaprc.ff12SB) [41]. The force field of the ligand **TC6** was derived using the restrained electrostatic potential (RESP) method. The ligand was first optimized using Gaussian 09 at HF/6-31G* level of theory and the partial atomic charges were fitted using the R.E.D package [42]. The simulation was carried out in explicit solvent of an orthorhombic box of TIP3P water molecules such that no solute atoms was within 8 Å from any side of the box [43]. The tLeap module of Amber 15 was used to add hydrogen atoms and counter ions Cl⁻ (three atoms) and Na⁺ (two atoms) were added for neutralization of MAO-A and MAO-B respectively. The long range electrostatic potential was calculated by using Partial Mesh Ewald (PME) method with a direct space and vdW cut-off of 12 Å [44].

Each of the systems was minimized twice, first with initial minimization for 1000 steps (500 steepest descent followed by 500 steps of conjugate gradient) with strong constrained on both ligands and the protein while the second minimization was for 100 steps with no constrain. This was followed by a canonical ensemble MD simulation where the systems were gradually heated up to temperature of 300.00 K for a simulation steps of 25,000 using Langevin thermostat with a collision frequency of 1.0 ps⁻¹ and a harmonic restrained of 5 kcal/mol Å was applied on the solutes. This was followed by another 25,000 steps of NPT simulation to control the density of the systems and 250,000 steps of equilibration at 300.00 K temperature, 1 bar pressure and a coupling constant of 2 ps. Thereafter, the production MD was carried out and the frame was recorded at every 500 steps of simulation and a time step of 2 fs was used all through the MD. All bond lengths involving hydrogen atoms were restrained using SHAKE algorithm [45].

The package BIO3D was used for the analysis of the conformational changes in the trajectory of the protein while the secondary structures were predicted using DSSP [46]. The visualization of the results was done using VMD, Chimera, Pymol and Ligplus [47-50]. The change in the binding free energy of the systems from their

unbound state to bound state was calculated using Poisson Boltzman (MM-PBSA) and Generalized Born (MM-GBSA) methods [51-54]. Both the GBSA and PBSA binding energy of the two systems were computed using a total of 1000 snapshots taken from 10000 ps of MD trajectory at 10 ps intervals. The binding free energy can be represented with the equation (1):

$$\Delta G_{bind}^0 = \Delta G_{Gas, complex}^0 + \Delta G_{solv, complex}^0 - [\Delta G_{receptor}^0 + \Delta G_{ligand}^0] \quad (1)$$

Solvation free energies were calculated as contribution from electrostatic by either solving the linearised Poisson Boltzman (G_{PB}) or Generalized Born equation (G_{GB}) with addition of empirical term for hydrophobic contributions (G_{SA}). The G_{SA} can be calculated from the solvent accessible surface area (SASA) equation (2).

$$\Delta G_{solv}^0 = \Delta G_{elect, \epsilon=80}^0 - \Delta G_{elect, \epsilon=1}^0 + \Delta G_{hydrophobic}^0 \quad (2)$$

The free energy in vacuum can be approximated as the average interaction energy between receptor and ligand, and putting the entropy change upon binding into consideration if desired equation (3).

$$\Delta G_{Gas}^0 = \Delta E_{MD}^0 - T \cdot \Delta S_{NMA}^0 \quad (3)$$

3. Results and Discussion

3.1. Chemistry

The chlorinated chalcone (**TC1-TC11**) derivatives were efficiently synthesized according to the pathway shown in Scheme 1. The chemical structures of the compounds have been characterized by means of their ¹H NMR, ¹³C NMR, mass spectroscopic datas and elemental analysis. ¹H-NMR spectrum showed different types of protons corresponding to the signals of α - β unsaturated unit, chlorine substituted thiophene and the mono substituted phenyl system. It has been noted that, the up field proton of α -carbon and down field proton of β -carbon coupled with methine proton with coupling constants (15.2-15.8 Hz). This suggests the presence of trans configuration in the chlorinated thienyl chalcones. The protons belonging to the to the aromatic ring and thiophene ring are observed with the expected chemical shift and integral value. ¹³C NMR displayed carbonyl carbon of (**TC1-TC11**) between δ 180.53–181.82. The characteristic peaks were observed in the mass spectra of the synthesized compounds. The presence of chlorine atom in all the compounds showed a characteristic [M+2] isotope peaks. The presence of [M+4] isotope peak in compound **TC8** clearly showed the presence of two chlorine atoms.

3.2. Biochemistry

3.2.1. MAO inhibition studies

Taking into the account of previous studies of chalcones on MAO inhibition, our current work is focused on modifying the molecular structure of very potent MAO-B inhibitors by introducing new functional groups at the para position on the **B** ring of chlorinated thienyl chalcones to improve their activities. All the newly synthesized compounds were investigated for their potential hMAO inhibitory activity using recombinant hMAO-A and hMAO-B. Enzyme activities were determined by a fluorimetric method using the Amplex Red MAO assay kit. Novel compounds and reference inhibitors (moclobemide, selegiline and lazabemide) were treated with Amplex Red reagent, and it was shown that the test compounds did not interfere with the measurements. Test compounds either did not interact with resorufin since the fluorescence signal did not change when the test and reference compounds were treated with various concentrations of resorufin. The inhibition constant (K_i) and selectivity indexes (SI) of the titled compounds are depicted in the Table 1. Specific enzyme activities were calculated as 169.33 ± 8.98 pmol/mg/min ($n=3$) for hMAO-A and 140.22 ± 6.05 pmol/mg/min ($n=3$) for hMAO-B.

With the exception of **TC7**, which was a selective MAO-A inhibitor, all derivatives inhibited hMAO-B potently and selectively with competitive mode of inhibition and some structure-activity relationships (SARs) were inferred from the data of enzymatic experiments. The most potent compound **TC6** with an ethyl group at the *para* position on the phenyl system showed the best activity and higher selectivity towards hMAO-B with K_i and SI values of 0.31 ± 0.02 μ M and 16.84. Among the synthesized chlorinated thiophene chalcones, presence of lipophilic electron donating groups such as ethyl, methyl, methoxyl and dimethylamino groups at the *para* position on the phenyl ring were found to be selective towards the inhibition of MAO-B. Presence of halogen such as chlorine and bromine atoms were also showed favourable activity towards MAO-B. Introduction of deactivating nitro group shifted potent and selective towards MAO-A with a K_i value of 0.49 ± 0.02 μ M. By analysing hMAO-B inhibition potencies of the chlorinated thiophene chalcones derivatives, it is clear that electron donating substitutions at the *para* position on the phenyl ring is preferable over substitutions with electron withdrawing nitro and trifluoromethyl groups. The following order of MAO inhibitory activity was observed for the chlorinated thienyl chalcones:

hMAO-A: 4-NO₂ > 4-Br > 4-Cl > 4-N-(CH₃)₂ > 4-CH₃ >> 4-F > 4-OCH₃ > 4-H > 4-CF₃ > 4-C₂H₅ > 4OH

hMAO-B: 4-C₂H₅ > 4-N-(CH₃)₂ > 4-CH₃ > 4-OCH₃ > 4-Br > 4-Cl > 4-H > 4-OH > 4-CF₃ > 4-F > 4-NO₂

3.2.2. Kinetic studies

Kinetic analyses were carried out for most potent MAO-B inhibitor **TC6** from this series. The purpose of this experimentation was to ascertain the mode of MAO-B inhibition by chlorinated thienyl chalcones. A set of

Lineweaver-Bruke plots were constructed in the absence and presence of various concentrations of compound **TC6**. The observation that the lines were linear and intersects on the y-axis suggests that **TC6** interacts with the catalytic site of hMAO-B, with a competitive mode of inhibition (fig. 2). The replot of the slopes versus inhibitor concentration is shown in (fig. 3) and the K_i was estimated as 0.31 μM for **TC6**.

3.2.3. Reversibility studies

Reversible MAO-B inhibitors have significant advantages over the irreversible inhibitors for the management of Parkinson's disease [7]. Taking into the advantage of this drug design aspect, the goal of our study is to design and development of some new class of reversible type of MAO-B inhibitors. All tested synthesised compounds inhibited the hMAO isoforms reversibly. Table 2 presents the reversibility of hMAO-B inhibition with the novel compounds. The reversibility of MAO inhibition by the new derivatives was investigated by measuring the recoveries of MAO activities after dialysis of enzyme-inhibitor mixtures. MAO isoforms were incubated in the presence of the representative inhibitors, at concentrations equal to $5 \times \text{IC}_{50}$, for a period of 15 min and subsequently dialysed for 24 h. As shown in Table 2, MAO-B inhibition by compound **TC6** is completely reversed after 24 h of dialysis. As shown in the table 2, after similar preincubation and dialysis of MAO-B with the irreversible inhibitor selegiline, the enzyme action was not retrieved. Results suggest that the **TC** series are reversible inhibitors of hMAO and have considerable advantages compared to irreversible inhibitors which may possess serious pharmacological side effects.

3.3. Cytotoxicity studies

In vitro cytotoxicity of the synthesized compounds is tested in Hep2 cells at three different concentrations (1–100 μM). The results showed that all the compounds presented in the current study are completely non-toxic with 74–88 % viable cells to hepatic cells at 100 μM concentration. At 10 μM , only the difference between the % viability values of the compounds **TC5**, **TC7** and **TC11** were found to be statistically significant at $p > 0.05$ (Table 3).

3.4. Molecular docking studies

Several researchers preferred to use the PDB of MAO co-crystallized with noncovalent ligands (2Z5X, 2V60, 2BK3) [55, 56] for molecular docking studies. The recent report of Badavth *et al.*, suggested that the experimental and predicted (Estimated K_i value) values did not correlate well with these [57]. Hence, we adopted the earlier protocol reported by our group with 2BXR and 2BYB [58].

The 5-chloro thiophene nucleus of **TC6** is located within the substrate cavity of the MAO-B enzyme, in close proximity of the FAD cofactor (Fig. 4). Since the entrance cavity is reported to be a highly hydrophobic space, it may be expected that an enhancement of the lipophilicity of the ethyl substitution on ring **B** in chlorinated thienyl chalcone will result in more productive Van der Waals interactions with the entrance cavity, and thus an enhancement in binding affinity. This may as well explain the observed enhancements of MAO-B inhibition potency of **TC6** compared to the unsubstituted homologue **TC1**.

The details of the component energies of all the ligands towards the active site of MAO-A and B are presented in table 4. This revealed a factor that an increase in the VdW energy of the ligands showed increase in potency as well as selectivity toward hMAO-B [58]. Compound **TC6** was found to be the most potent MAO-B inhibitor among the series with VdW energy of -10.44. The binding interaction of **TC6** is majorly stabilized by the π - π stacking interaction between the ethyl substituted phenyl ring and the aromatic ring of Tyr-435.

3.5. Molecular dynamics study

3.5.1. Binding energy analysis

Molecular dynamics study is a very important tool to understand the stability and the binding mode of the ligand-receptor interactions. It also helps to understand the dynamics of the protein, which represent the true nature of protein better than ordinary docking, which does not completely consider the dynamic of protein. In addition to normal molecular dynamics, we employed all-atom enhanced sampling method of accelerated molecular dynamics (AMD) in order to understand the possible rare events that can take place in the interaction of the ligand **TC6** with the two receptors after a much longer molecular dynamics [59]. AMD is an important method, because of the ability to accelerates and extends the time scale in molecular dynamics simulations through addition of a bias potential to the true potential such that will enhance the escape rates from potential wells. This method has been successfully applied to investigate conformational changes in proteins that typically occur on the millisecond time scale [60].

The root means square displacement (RMSD) of the protein backbone residues during the course of molecular dynamics (MD) and the changes in the potential (EPTOT) energy of the complexes MAO-A-**TC6** and MAO-B-**TC6** are shown in Fig. 5. The RMSD of the two complexes shows that stable conformational changes where obtained for both complexes during the normal MD and AMD methods. The total potential energy plots for normal and AMD are within the same range and have similar feature which is an indication that the

accelerated molecular dynamics does not change the potential surface of the systems. The EPTOT plot of MAO-A is characterized with higher energy level compare to MAO-B. The conformational changes in complex MAO-B is more significant compare to complex MAO-A which are characterized with higher and lower RMSD respectively.

The results from the MM-PBSA and its complementary MM-GBSA method for the binding analysis of ligand **TC6** with MAO-A and MAO-B are shown in Table 1. The two methods of binding studies show that **TC6** have stronger affinity for MAO-B than MAO-A during the normal MD which completely agrees with the experimental result. However, during the AMD, a significant decrease in the interacting free energy was obtained compare to normal MD and only MM-GBSA shows a better interaction of **TC6** with MAO-B compare to MAO-A (Table 1 and Fig. 6) while MM-PBSA completely disagree with experimental result. The favourable interaction of **TC6** with MAO-B is from the higher change ΔE_{elec} and ΔG_{gas} . As estimated from MM-GBSA, the difference in the binding free energy of the interaction of **TC6** with MAO-B compare to MAO-A is -5.474 kcal/mol in normal MD and -1.624 kcal/mol in AMD. Since AMD simulation method is able to account for the possible rare events of the protein complex, the significant decrease in the activities of the **TC6** interacting with both MAO-A and MAO-B is an indication of possible reduction in the efficiency of **TC6** as a limiting factors that can arise from huge conformational changes of the receptor. The decomposition of changes in the binding energy base on the residual contribution is shown in Table 2. As observed in residue decomposition for the interaction of **TC6**-MAO-A, the first five residues which were ranked during the normal MD to have the highest energy change (ILE 165, ASN 166, PHE 193, TYR 389, and TYR 426) are also ranked as top five in its AMD but not in the same order. In **TC6**-MAO-B, only three residues GLN 205, TYR 397 and TYR 434 out of the first five that were ranked during the normal MD to have the highest energy contribution to binding were also ranked during the AMD.

3.5.2. Study of conformational changes

An insight into the structural distribution and the conformational changes during the MD was obtained using the principal components analysis (PCA) which is orthogonal eigenvectors. The PCA is very significant because it gives special insight into the dynamics and conformational changes in both MAO-A and MAO-B as shown in

Fig. 7a. The average structures for the three predicted conformational changes based on the PCA analysis of the normal MD are shown in Fig. 7b. The average geometries of the three groups of conformations clearly show that the changes are predominantly the loop region of the receptors (7b). The region of the PCA that has the lowest energy are represented are circled round in the plot of changes in the potential energy (7c). The first three PC (PC-1, PC-2 and PC-3) captured 39% in MAO-A but 41.4% in MAO-B of the total variance in MD trajectory of the complexes. During the MD, a periodic jump in the conformation was observed for the complexes as clearly shown by the continuous colour scale of the PC from blue to red to green but there is no significant conformational change of α -helices and β -helices two protein backbones. This is more significant changes in the binding position of **TC6** from the averages geometries of the three clusters of conformations for MAO-A compare to MAO-B as suggested from PCA analysis (Fig. 7). The highest value for the residual fluctuations from the PCA analysis for normal MD for MAO-A was a little above 0.12 while that of MAO-B was a little above 0.15 which is a clear indication that that there is overall more residual conformational change in MAO-B compare to MAO-A.

Using the results from the AMD, the conformational changes of complexes MAO-A and MAO-B are shown in the Fig. 8 and 9 respectively. Both the root means square fluctuation (RMSF) and the PCA (PC1 and PC2) show the high level of residual fluctuations in MAOA are in the region 200-250 residues while in MAOB are found in the region 450-495 residues. The three predicted conformational changes are show in black, red and green colour (8c and 9c). The free energy surface was constructed using python script for reweighting of AMD simulations (8e and 9e) and also from change in the potential energy (8f and 9f) [61]. The two free energy surfaces clearly shown that the best conformation for MAO-A corresponds to black colour region of PCA while that of MAO-B correspond to green region. The structural comparisons of the best conformation in MAO-A and MAO-B during the AMD with that of normal M-D are shown in Fig. 10.

The observed conformational changes in MAO-A are mainly loop region while it involves both the α -helices and loop in MAO-B. Also higher levels of hydrophobic interactions are observed in the ligand interaction with MAO-B compare to MAO-A (10a and 10b). The results suggest that complex **TC6**-MAO-B is prone to higher conformational changes as a possible rare event than complex **TC6**-MAO-A (Fig. 10) which is also supported with more significant reduction in its interacting energy compare to MAO-A during the AMD (Table 5). This is further supported from the observed higher values of RMSF (≈ 4.0 , Fig. 9a), PC1 and PC2 residual fluctuations (≈ 0.25 , Fig. 9b) and the fluctuation of the three groups of predicted conformational changes (≈ 3.5 , Fig. 9d) for

the **TC6-MAO-B** interaction compare to what was observed for the corresponding parameters in Fig. 8 for the interaction of **TC6-MAO-A**.

The residue-residue correlation plots were obtained by computing dynamical cross-correlation matrix (DCCM) according to the following equation (4) [62].

$$C(i, j) = \frac{c(i, j)}{c(i, i)^{1/2} c(j, j)^{1/2}} \quad (4)$$

The ‘C(i,j)’ represent the covariance matrix element of protein fluctuation between residues ‘i’ and ‘j’. The plots of the dynamical cross-correlation motions (DCCM) for the **TC6-MAO-A** and **TC6-MAO-B** are shown in Fig. 11 and their graphical representation in 3D showing only the most significant networks of correlation and anticorrelation ($|C(i,j)| \geq 0.6$). In the two complexes, most of the observed DCCM especially for $|C(i,j)| \geq 0.7$ were mainly from the neighbouring residues (intradomain correlation) that form a secondary structure while very few were from distant amino acids belonging to different regions or domains (interdomain correlation). A higher level of locally coupled motions was observed for the α -helices and β -helices residues with their surroundings compare to the loop region. Both **TC6-MAO-A** and **TC6-MAO-B** show a significant level of correlation but a higher networks of correlation was observed for **TC6-MAO-B** compare to **TC6-MAO-A**. Also, **TC6-MAO-A** show a significant level of anticorrelation (blue lines) during the dynamics of its atoms which was found to be between the β -sheet and the loop.

The molecular dynamic simulation shows a better interaction of **TC6** with **MAO-B** compare to **MAO-A**. This is confirmed from the results of the binding free energy using MM-PBSA and MM-GBSA during the normal MD but only MM-GBSA confirms this observation during the AMD simulation. Using AMD to study the possible rare events in the complexes, the results suggest that complex **TC6-MAO-B** is prone to a more significant conformational changes than **TC6-MAO-A** which can significantly reduce the binding affinity of the inhibitor. The molecular dynamics of the two complexes also give further information about the differences in binding mode of **TC6**. Some of the observed differences in binding of **TC6** to **MAO-A** compare to **MAO-B** are reduction in the size of binding site, higher RMSD of the protein backbone residues, stronger fluctuation of the potential energy, higher values of the RMSF and PCA of the residues though over lower range of residues. These properties are clear indication that the binding of **TC6** to **MAO-A** is weaker compare to its binding with **MAO-B**.

4. Conclusion

The present study discovers a number of potent new MAO-B inhibitors among the heterocyclic chlorinated thiophene based chalcone class of compounds. Experimental results further revealed that all the heterocyclic chalcones under the present study are reversible type MAO inhibitor. The molecules here reported may be considered promising hit compounds for the discovery of new neuroprotectants and for the development of multi-target directed ligands having MAO-B inhibition as the core activity. The finely tuned exploration of the various groups at the para position on the ring **B** of chlorinated chalcone allowed a precise development of a new class of MAO-B inhibitors. The lead chalcones can be further optimized for the preparation of 2-pyrazolines, a promising structural scaffold for the development of inhibitors of MAO-A and B.

Acknowledgements

The authors thankful to IIRBS, Mahatma Gandhi University, Kottayam, India and SAIF-IIT, Chennai for carrying out the spectral analysis. The authors also thanks to the School of Pure & Applied Physics, M.G. University, Kottayam, India for X-ray diffraction analysis.

References

- [1] R.H. Haung, R. Faulkner, *J. Biol. Chem.* 256 (1981) 9211–9215.
- [2] J.C. Shih, K. Chen, M.J. Ridd, *Annu. Rev. Neurosci.* 22 (1999) 197-217.
- [3] M. Yamada, H. Yasuhara, *Neurotoxicology* 25 (2004) 215–221.
- [4] D.E. Edmondson, *Curr. Pharm. Des.* 20 (2014) 155-160.
- [5] J.M. Andrews, C.B. Nemeroff, *Am. J. Med. Chem.* 97 (1994) 24S-32S.
- [6] B. Drukarch, F.L. van Muiswinkel, *Biochem. Pharmacol.* 59 (2000) 1023–1031.
- [7] S. Carradori, R. Silvestri, *J. Med. Chem.* 58 (2015) 6717-6732.
- [8] S. Tanaka, Y. Kuwai, M. Tabata, *Planta Med.* 53 (1987) 5-8.
- [9] H. Haraguchi, Y. Tanaka, A. Kabbash, T. Fujioka, T. Ishizu, A. Yagi, *Phytochemistry* 65 (2004) 2255–2260.
- [10] X. Pan, L. D. Kong, Y. Zhang, C. H. Cheng, R. X. Tan, *Acta Pharmacol. Sinica* 21 (2000) 949–953.
- [11] F. Chimenti, R. Fioravanti, A. Bolasco, P. Chimenti, D. Secci, F. Rossi, M. Yanez, F. Orallo, F. Ortuso, S. Alcaro, *J. Med. Chem.* 52 (2009) 2818-2824.
- [12] S.J. Robinson, J.P. Petzer, A. Petzer, J.J. Bergh, A.C.U. Lourens, *Bioorg. Med. Chem. Lett.* 23 (2013) 4985-4989.

- [13] G. Jo, S. Ahn, B.G. Kim, H.R. Park, Y.H. Kim, A.H. Cho, D. Koh, Y. Chong, J.H. Ahn, Y. Lim, *Bioorg. Med. Chem.* 21 (2013) 7890-7897.
- [14] N. Morales-Camilo, C.O. Salas, C. Sanhueza, C. Espinosa-Bustos, S. Sepúlveda-Boza, M. Reyes-Parada, F. Gonzalez-Nilo, A. Fierro, *Chem. Biol. Drug Des.* 85 (2015) 685-695.
- [15] S. Zaib, S.U.F. Rizvi, S. Aslam, M. Ahmad, S.M.A. Abid, M. al-Rashida, J. Iqbal, *Med. Chem.* 11 (2015) 580-589.
- [16] S. Zaib, S.U.F. Rizvi, S. Aslam, M. Ahmad, M. al-Rashida, J. Iqbal, *Med. Chem.* 11 (2015), 497-505.
- [17] B. Mathew, G.E. Mathew, G. Uçar, I. Baysal, J. Suresh, J. K. Vilapurathu, A. Prakasan, J. K. Suresh, A. Thomas, *Bioorg. Chem.* 62 (2015) 22-29.
- [18] B. Mathew, G. Uçar, S. Yabanoğlu-Çiftçi, I. Baysal, J. Suresh, G.E. Mathew, J.K. Vilapurathu, A.M. Nadeena, P. Nabeela, V. Lakshmi, A. Haridas, F. Fathima, *Lett. Org. Chem.* 12 (2015) 605-613
- [19] J.W. Choi, B.K. Jang, N. Cho, J.H. Park, S.K. Yeon, E.J. Ju, Y.S. Lee, G. Han, A.M. Pae, D.J. Kim, K.D. Park, *Bioorg. Med. Chem.* 23 (2015) 6486-6496.
- [20] C. Minders, J.P. Petzer, A. Petzer, A.C.U. Lourens, *Bioorg. Med. Chem. Lett.* 25 (2015) 5270-5276.
- [21] A. Hammuda, R. Shalaby, S. Rovida, D. E. Edmondson, C. Binda, A. Khali, *Eur. J. Med. Chem.* 114 (2016) 162-169.
- [22] B. Mathew, A. Haridas, G. Uçar, I. Baysal, M. Joy, G.E. Mathew, B. Lakshmanan, V. Jayaprakash, *ChemMedChem.* (2016).doi:10.1002/cmdc.201600122.
- [23] S. Carradori, M. D'Ascenzio, P. Chimentì, D. Secci, A. Bolasco, *Mol. Divers.* 18 (2014) 18:219-243.
- [24] B. Mathew, A. Haridas, J. Suresh, G.E. Mathew, G. Uçar, V. Jayaprakash, *Cent. Nerv. Syst. Agents Med. Chem.* (2016) doi:10.2174/1871524915666151002124443.
- [25] G.M. Sheldrick, *Acta Cryst. C* 71 (2015) 3-8.
- [26] L.G. Farrugia, *J. Appl. Cryst.* 45 (2012) 849-854.
- [27] A.L. Spek, *Acta Cryst. D* 65 (2009) 148-155.

- [28] M.C. Anderson, F. Hasan, J.M. McCrodden, K.F. Tipton, *Neurochem. Res.* 18 (1993) 1145–1149.
- [29] F. Chimenti, E. Maccioni, D. Secci, A. Bolasco, P. Chimenti, A. Granese, S. Carradori, S. Alcaro, F. Ortuso, M. Yáñez, *J. Med. Chem.* 51 (2008) 4874–4880.
- [30] M. Yáñez, N. Fraiz, E. Cano, F. Orallo, *Biochem. Biophys. Res. Commun.* 344 (2006) 688–695.
- [31] M.M. Bradford, *Anal. Biochem.* 72 (1976) 248–254.
- [32] F. Chimenti, S. Carradori, D. Secci, A. Bolasco, B. Bizzarri, P. Chimenti, A. Granese, M. Yáñez, F. Orallo, *Eur. J. Med. Chem.* 45 (2010) 800–804.
- [33] M.B. Hansen, S.E. Nielsen, K. Berg, *J. Immunol. Meth.* 119 (1989) 203–210.
- [34] C.F. Wu, R. Bertorelli, M. Sacconi, G. Pepeu, S. Consolo, *Neurobiol. Aging*, 9 (1988) 357–361.
- [35] G.M. Morris, R. Huey, W. Lindstrom, M.F. Sanner, R.K. Belew, D.S. Goodsell, A.J. Olson, *J. Comput. Chem.* 30 (2009) 2785–2791.
- [36] L. De Colibus, M. Li, C. Binda, A. Lustig, D.E. Edmondson, A. Mattevi, *Proc. Natl. Acad. Sci. USA* 102 (2005) 12684–12689.
- [37] B.V. Nayak, S. Ciftci-Yabanoglu, S.S. Jadav, M. Jagrat, B.N. Sinha, G. Ucar, V. Jayaprakash, *Eur. J. Med. Chem.* 69 (2013) 762–767.
- [38] A.W. Schuttelkopf, D.M. van Aalten, *Acta Crystallogr. D Biol. Crystallogr.* 60 (2004) 1355–1363.
- [39] B. Mathew, J. Suresh, S. Anbazhagan, *S. Dev. Biomed. Aging Pathol.* 4 (2014) 327–333.
- [40] A.W. Götz, M.J. Williamson, D. Xu, D. Poole, S. Le Grand, R.C. Walker, *J. Chem. Theory Comput.* 8 (2012) 1542–1555.
- [41] K. Lindorff-Larsen, S. Piana, K. Palmo, P. Maragakis, J.L. Klepeis, R.O. Dror, D.E. Shaw, *Proteins: Struct., Funct., Bioinf.* 78 (2010) 1950–1958.
- [42] F.V. Dupradeau, A. Pigache, T. Zaffran, C. Savineau, R. Lelong, N. Grivel, D. Lelong, W. Rosanski, P. Cieplak, *Phys. Chem. Chem. Phys.* 12 (2010) 7821–7839.

- [43] W.L. Jorgensen, J. Chandrasekhar, J.D. Madura, R.W. Impey, M.L. Klein, *J. Chem. Phys.* 79 (1983) 926–935.
- [44] U. Essmann, L. Perera, M.L. Berkowitz, T. Darden, H. Lee, L.G. Pedersen, *J. Chem. Phys.* 103 (1995) 8577–8593.
- [45] J.P. Ryckaert, G. Ciccotti, H.J. Berendsen, *J. Comput. Phys.* 23 (1977) 327–341.
- [46] B.J. Grant, A.P.C. Rodrigues, K.M. Elsayy, J.A. McCammon, L.S.D. Caves, *Bioinformatics*, 22 (2006), 2695-2696.
- [47] W. Humphrey, A. Dalke, K. Schulten. *J. Mol. Graph.* 14 (1996) 33–38.
- [48] E.F. Pettersen, T.D. Goddard, C.C. Huang, G.S. Couch, D.M. Greenblatt, E.C. Meng, T.E. Ferrin, *J. Comput. Chem.* 25 (2004) 1605–1612.
- [49] Schrodinger LLC. 2015. “The PyMOL Molecular Graphics System, Version 1.8.
- [50] R.A. Laskowski, M.B. Swindells, *J. Chem. Inf. Model.* 51 (2011) 2778-2786.
- [51] P.A. Kollman, I. Massova, C. Reyes, B. Kuhn, S. Huo, L. Chong, M. Lee, T. Lee, Y. Duan, W. Wang, *Acc. Chem. Res.* 33 (2000) 889–897.
- [52] I. Massova, P.A. Kollman, *Perspect. Drug Discovery Des.* 18 (2000) 113–135.
- [53] V. Tsui, D.A. Case, *Biopolymers*, 56 (2000) 275–291.
- [54] A. Onufriev, D. Bashford, D.A. Case, *J. Phys. Chem. B*, 104 (2000) 3712–3720.
- [55] F. Chimenti, A. Bolasco, D. Secci, P. Chimenti, A. Granese, S. Carradori, M. Yáñez, F. Orallo, F. Ortuso, S. Alcaro, *Bioorg. Med. Chem.* 18 (2010) 5715–5723.
- [56] N. Desideri, A. Bolasco, R. Fioravanti, L. Proietti Monaco, F. Orallo, M. Yáñez, F. Ortuso, S. Alcaro, *J. Med. Chem.* 54 (2011) 2155–2164.
- [57] V. N. Badavath, I. Baysal, G. Ucar, B. N. Sinha, V. Jayapraksh, *ACS Med. Chem. Lett.* 7 (2016) 56-61.
- [58] V. N. Badavath, I. Baysal, G. Ucar, S. K. Mondal, B. N. Sinha, V. Jayapraksh, *Arch. Pharm. Chem. Life Sci.* 349 (2016) 9–19.

- [59] D. Hamelberg, J. Mongan, J.A. McCammon, *J. Chem. Phys.* 120 (2004) 11919-11929.
- [60] L.C.T. Pierce, R.S. Ferrer, A.F. de Oliveria, J.A. McCammon, R.C. Walker. *J. Chem. Theory Comput.* 8 (2012) 2997-3002.
- [61] Y. Miao, W. Sinko, L. Pierce, D. Bucher, R.C. Walker, J.A. McCammon, *J. Chem. Theory Comput.* 10 (2014) 2677-2689.
- [62] P.H. Huenberger, A.E. Mark, W.F. van Gunsteren, *J. Mol. Biol.* 252 (1995) 492-503.

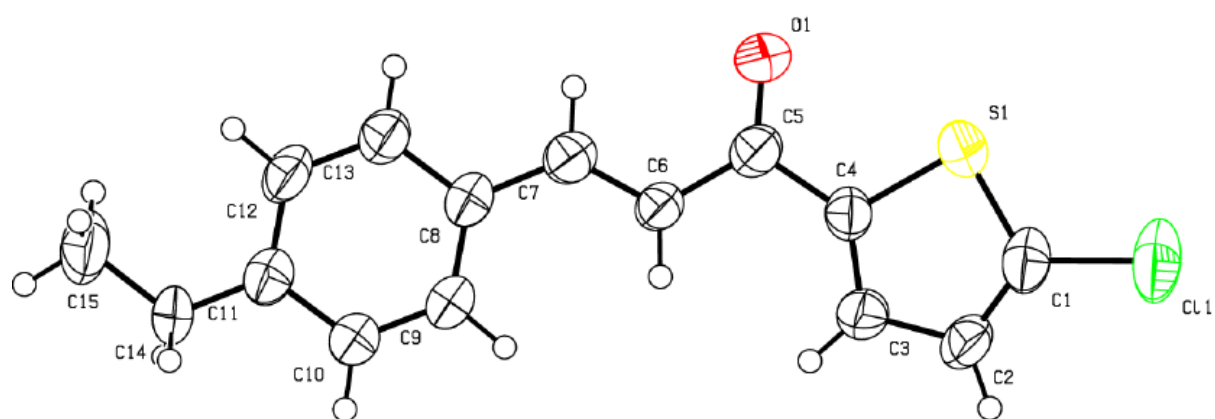


Fig 1. ORTEP diagram of compound TC6 [lead molecule]

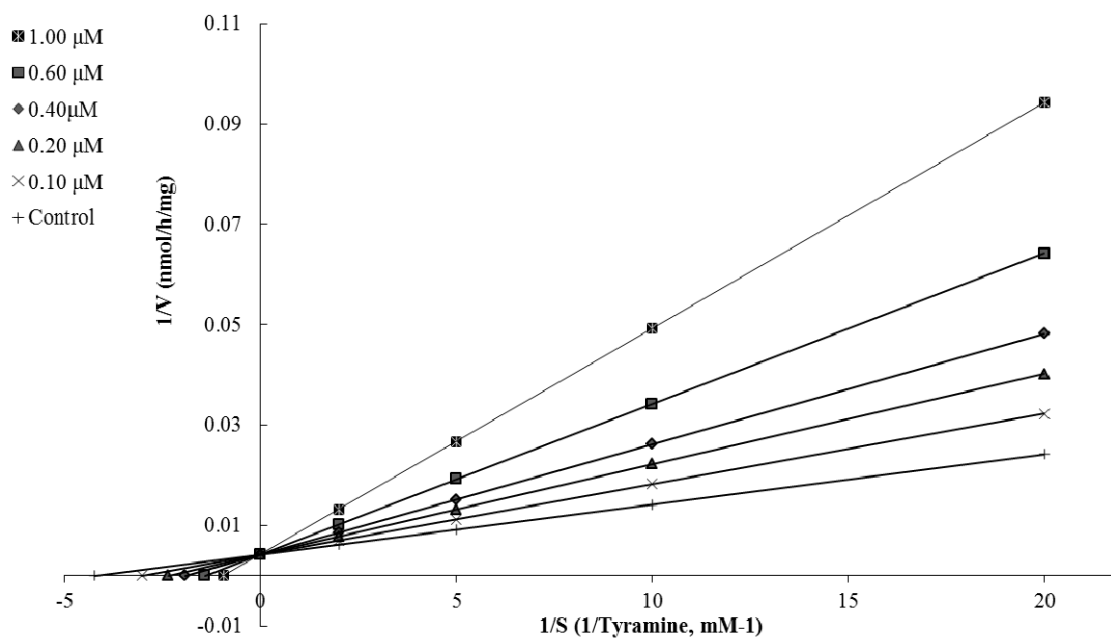


Fig.2. Lineweaver-Burk plots of hMAO-B activity in the absence and presence of various concentrations of compound TC6

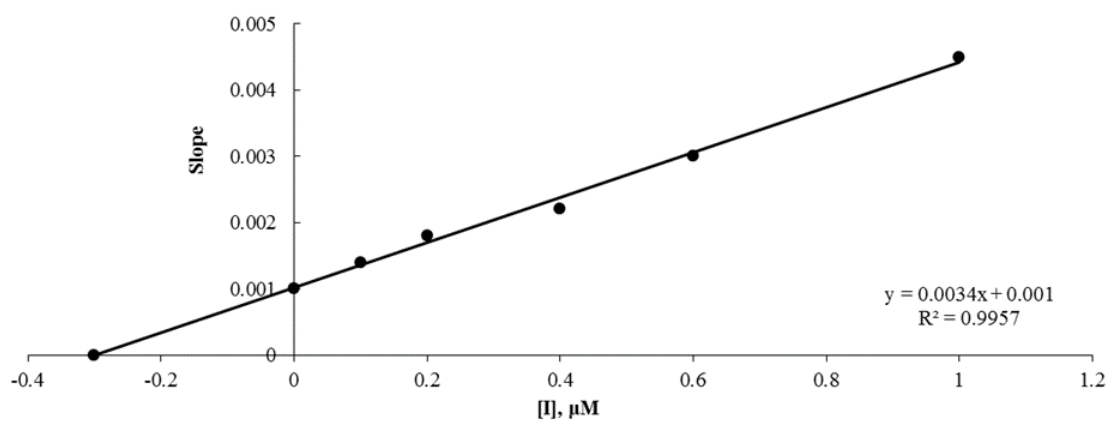


Fig. 3. The graph of the slopes of Lineweaver-Burk plots versus inhibitor concentrations. K_i was calculated as 0.31 μM

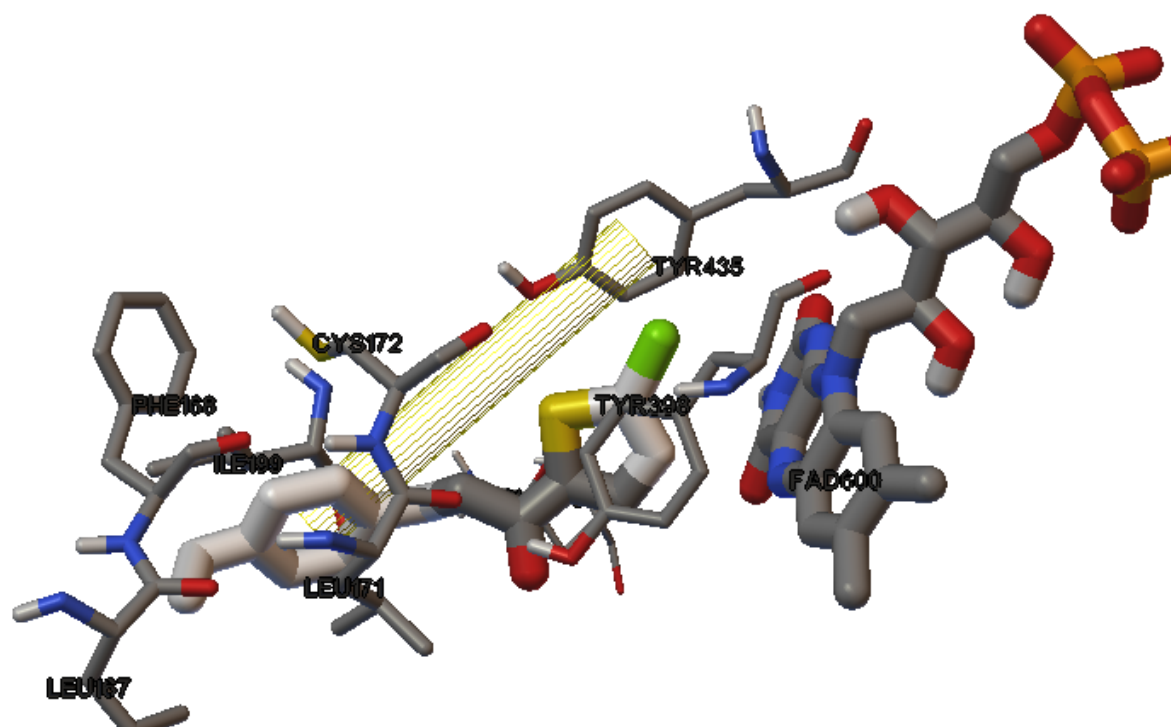


Fig. 4. Interaction of compound TC6 with the hMAO-B (PDB: 2BYB) active site: Yellow mesh indicates π - π stacking interaction

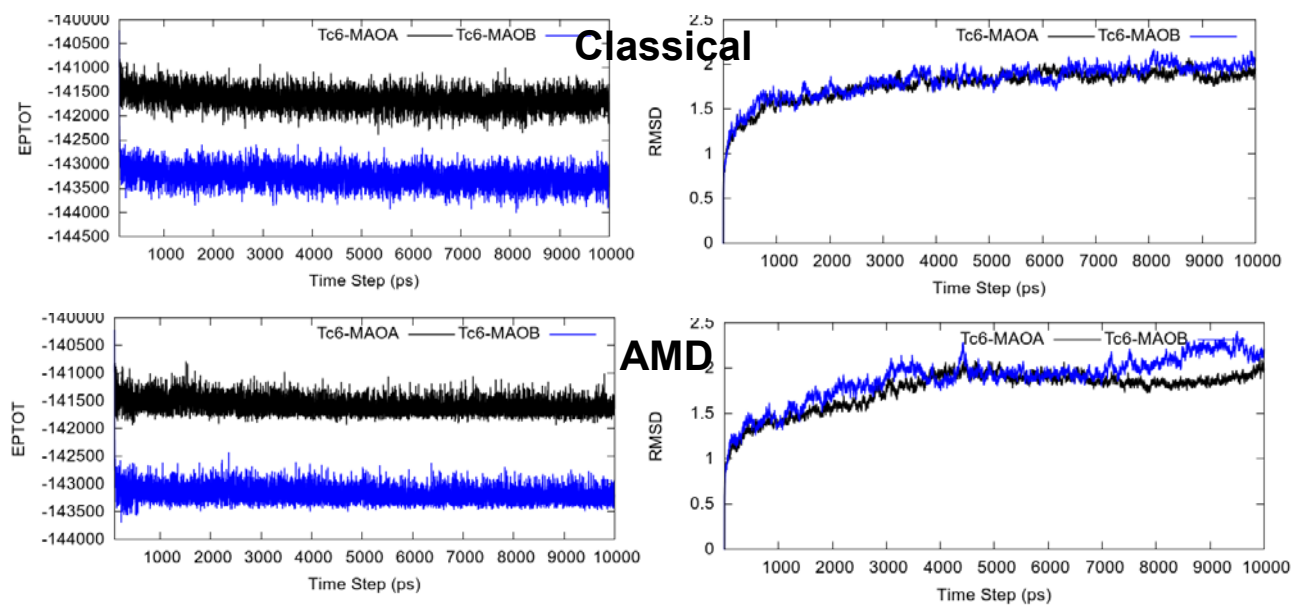


Fig. 5. The potential energy (EPTOT) and the RMSD of all the mass except hydrogen atoms obtained from the trajectories of the normal MD and AMD

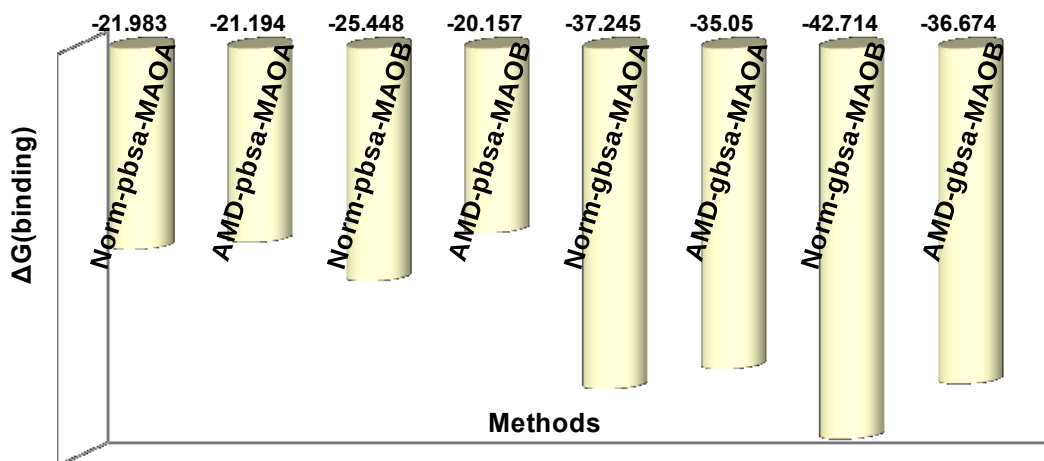


Fig. 6. The changes in the total free energy of the TC6 interaction with MAO-A and MAO-B using the MM-PBSA and MM-GBSA methods from the trajectory of the normal MD and AMD.

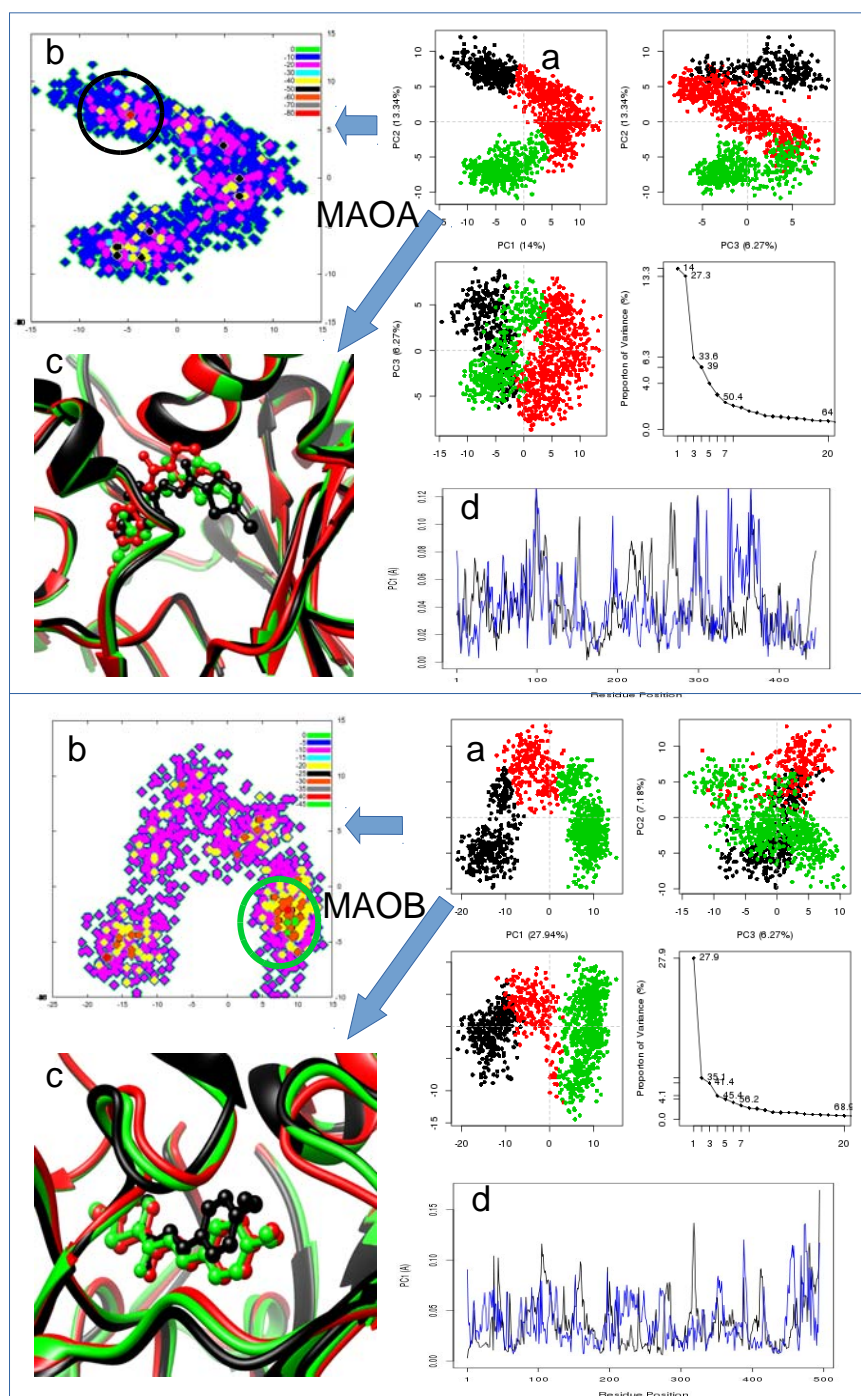


Fig. 7. The PC analysis of the complexes TC6-MAO-A and TC6-MAO-B showing (a) the features of the conformational changes during the normal MD, (b) change in potential energy of the conformation, (c) the geometries of the three group of conformations and (d) the residual fluctuation in the plane PC1 and PC2 from PCA analysis. The best conformations in terms of change in potential energy are shown in circle with colour corresponding to the group of their PCA colour.

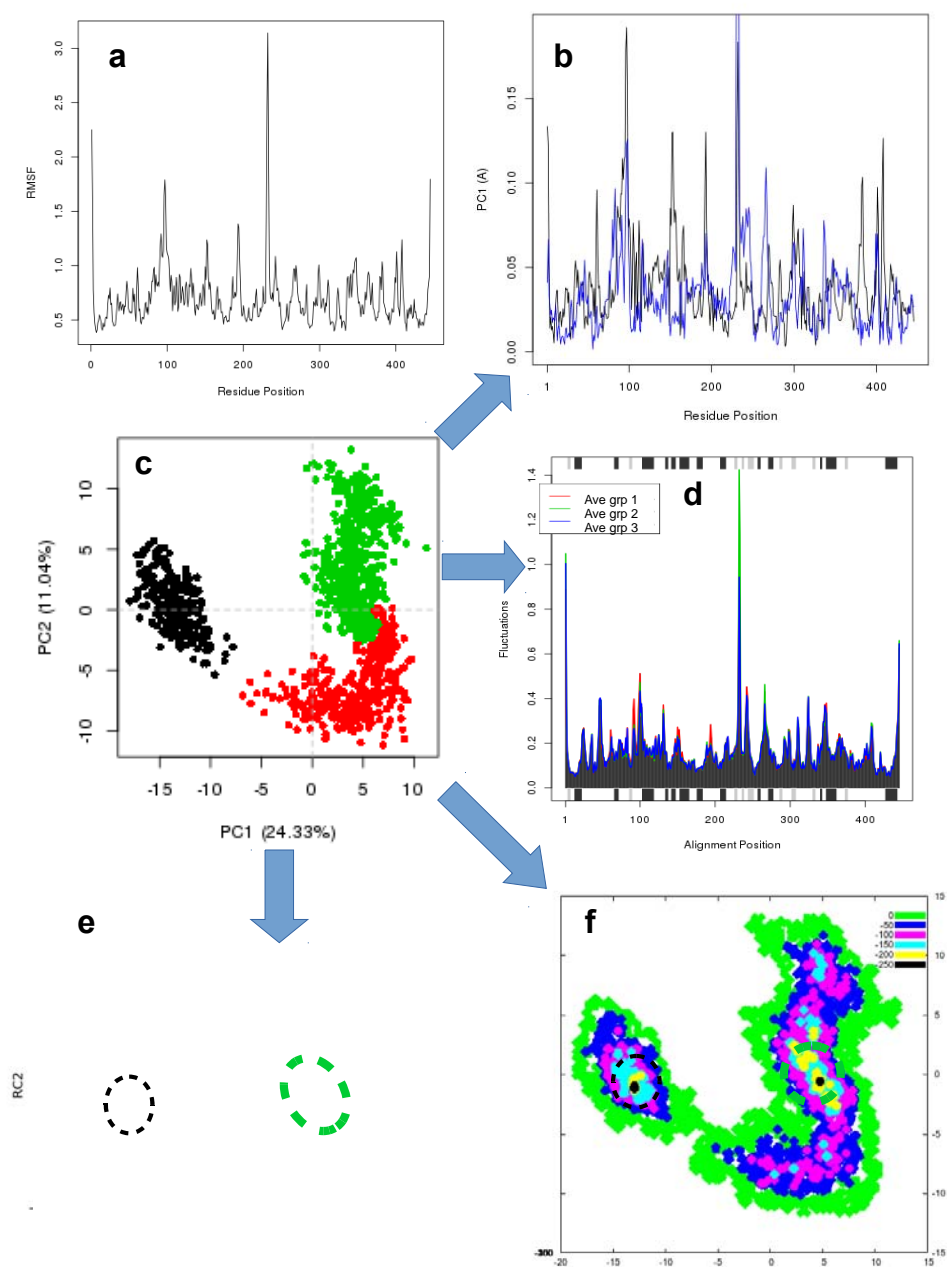


Fig. 8. The plots for the TC6-MAO-A interaction during the course of AMD showing (a) The root means square fluctuation of residues during the dynamics (b) The residue fluctuation in the PC1 and PC2, (c) the clusters of the three conformational changes in the PC1 and PC2 planes (d) the normal mode prediction of the fluctuation of the three groups of conformations (e) the potential energy surface plotted from reweighting of AMD and (f) the potential energy plotted from the change in the potential energy during the course of AMD from the initial value.

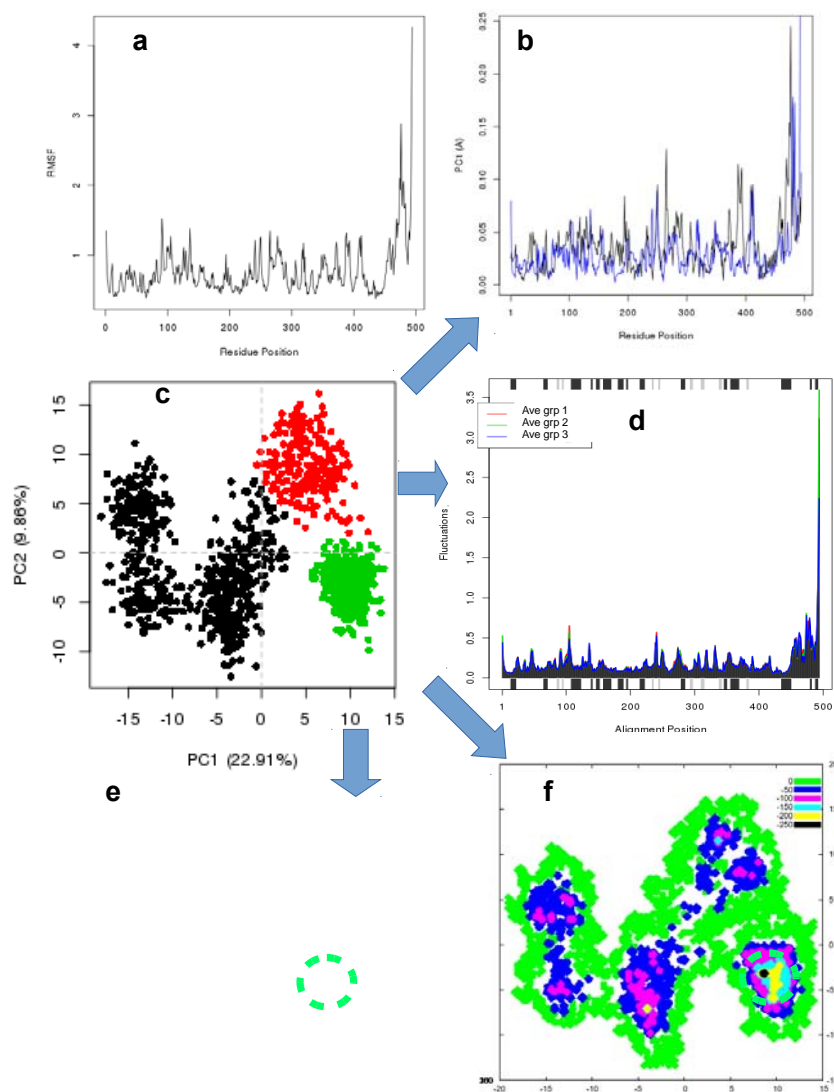


Fig. 9. The plots for the TC6-MAOB interaction during the course of AMD showing (a) The root means square fluctuation of residues during the dynamics (b) The residue fluctuation in the PC1 and PC2, (c) the clusters of the three conformational changes in the PC1 and PC2 planes (d) the normal mode prediction of the fluctuation of the three groups of conformations (e) the potential energy surface plotted from reweighting of AMD and (f) the potential energy plotted from the change in the potential energy during the course of AMD from the initial value.

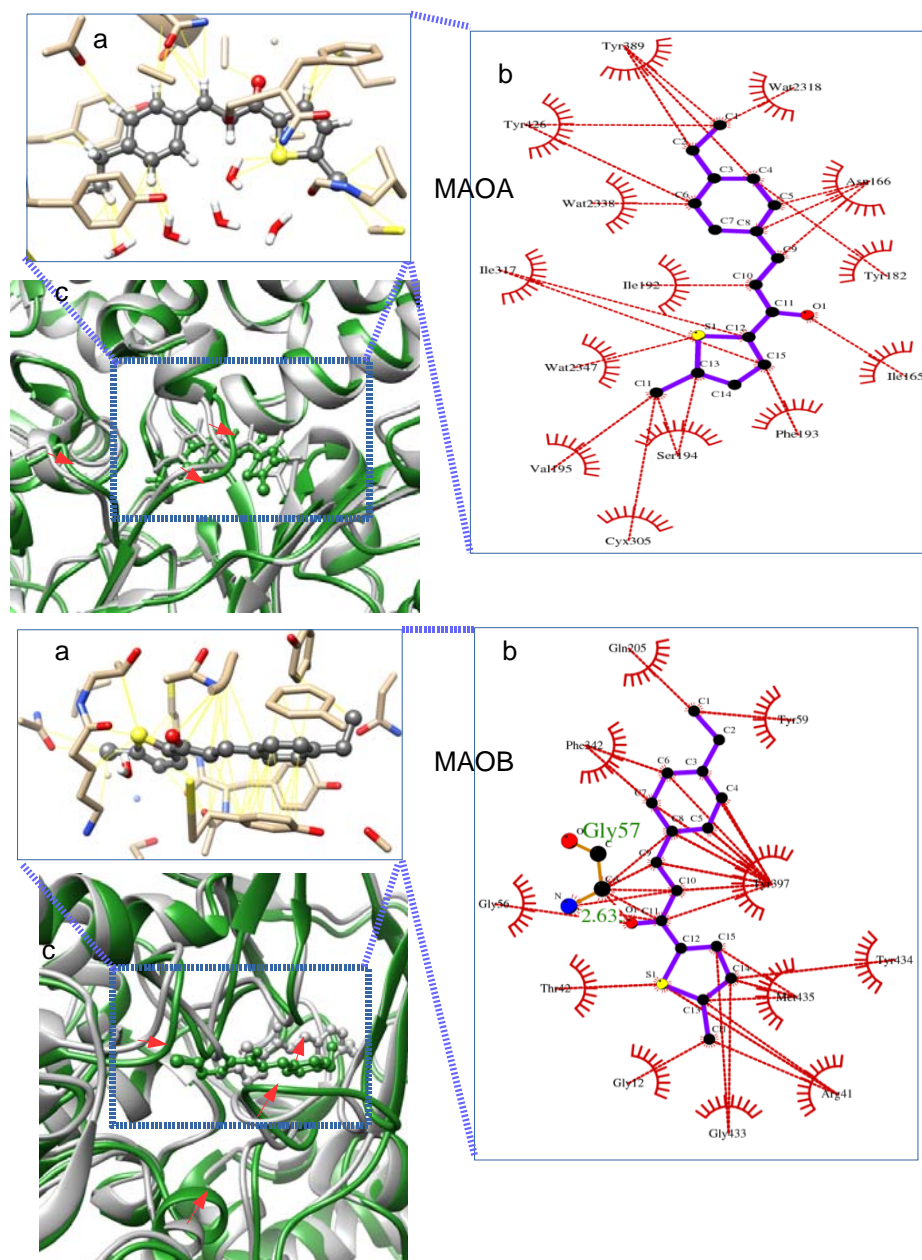


Fig.10. The structure of the interaction of TC6 with MAO-A (**1a-c**) and MAO-B (**2a-c**) showing the suggested best conformation from the AMD (green) compare to the normal (grey) and the binding site interaction with receptor residues (“a” and b”).

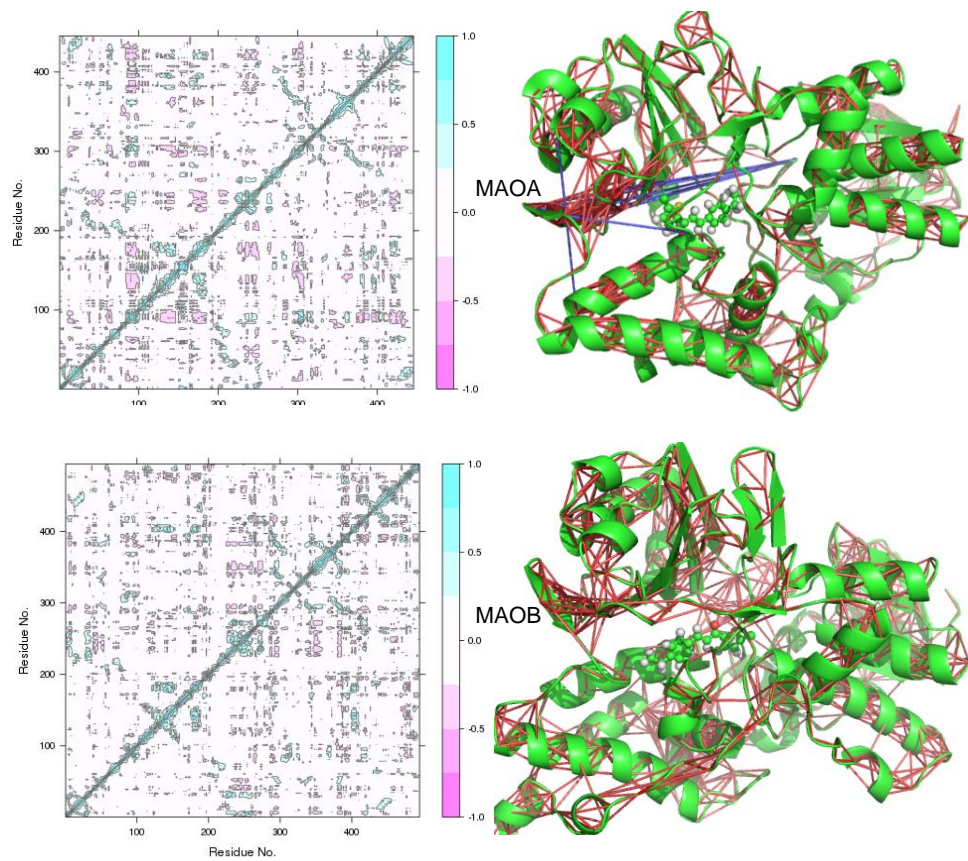
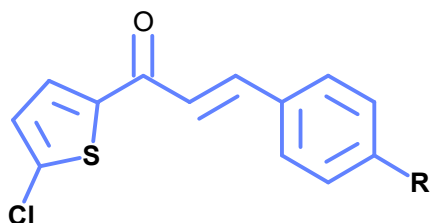


Fig.11. The residue-residue correlation (red line) and anti-correlation (blue lines) during the AMD estimated using the dynamical cross-correlation motions (DCCM) for the MAO-A and MAO-B with inhibitor

Table 1. hMAO inhibitory activities of chlorinated thiophene based chalcones

Compounds	R	Experimental K_i value (μM)*		Experimental SI**	Inhibition type	Reversibility	MAO selectivity
		MAO-A	MAO-B				
TC1	H	4.28±0.24	1.03±0.09	4.15	Competitive	Reversible	MAO-B
TC2	OH	5.52±0.29	1.16±0.10	4.76	Competitive	Reversible	MAO-B
TC3	OCH ₃	3.98±0.21	0.75±0.05	5.31	Competitive	Reversible	MAO-B
TC4	CH ₃	2.76±0.19	0.64±0.03	4.31	Competitive	Reversible	MAO-B
TC5	N(CH ₃) ₂	2.00±0.15	0.60±0.03	3.33	Competitive	Reversible	MAO-B
TC6	CH ₂ CH ₃	5.22±2.09	0.31±0.02	16.84	Competitive	Reversible	MAO-B
TC7	NO ₂	0.49±0.02	2.55±0.13	0.19	Competitive	Reversible	MAO-A
TC8	Cl	1.60±0.14	0.79±0.04	2.03	Competitive	Reversible	MAO-B
TC9	Br	1.36±0.09	0.70±0.04	1.94	Competitive	Reversible	MAO-B
TC10	F	3.90±0.22	1.99±0.12	1.96	Competitive	Reversible	MAO-B
TC11	CF ₃	4.70±0.34	1.88±0.12	2.50	Competitive	Reversible	MAO-B
Moclobemide	-	0.13±0.009	1.98±0.13	0.065	Competitive	Reversible	MAO-A
Selegiline	-	7.11±0.49	0.14±0.01	50.79	Suicide inhibitor	Irreversible	MAO-B
Lazabemide	-	880.40±33.00	0.006±0.001	146.73	Competitive	Reversible	MAO-B



*Values represent the mean±SEM of three independent experiments

**Selectivity index. It was calculated as $K_i(\text{MAO-A})/K_i(\text{MAO-B})$. Selectivity towards MAO-A increases as the corresponding SI decreases while selectivity towards MAO-B isoform increases as the corresponding SI increases.

Table 2. Reversibility of hMAO inhibition by chlorinated thiophene based chalcones

Compounds incubated with hMAO	hMAO-A activity before dialysis (%)	hMAO-A activity after dialysis (%)	hMAO-B activity before dialysis (%)	hMAO-B activity after dialysis (%)	Reversibility
With no inhibitor	100±0.00	98.22±6.43	100±0.00	98.90±6.32	
Moclobemide	33.20±1.75	98.74±4.13	90.11±5.03	97.55±4.23	Reversible
Selegiline	89.93±5.33	97.06±3.97	58.23±2.68	56.88±3.44	Irreversible
Lazabemide	92.00±4.61	98.03±4.22	7.00±0.56	89.11±5.03	Reversible
TC1	88.36±3.80	94.00±4.60	49.11±4.22	93.30±3.75	Reversible
TC2	85.00±3.29	93.55±3.20	48.20±2.17	93.00±4.55	Reversible
TC3	89.55±4.05	96.31±3.24	43.29±4.00	97.00±2.90	Reversible
TC4	90.00±4.60	97.12±2.05	40.22±2.95	92.00±2.26	Reversible
TC5	89.60±3.90	94.77±5.00	38.56±1.88	94.00±4.48	Reversible
TC6	82.90±4.66	93.22±4.60	32.03±1.95	97.10±4.55	Reversible
TC7	84.22±2.90	97.00±3.02	65.22±2.90	92.35±4.40	Reversible
TC8	88.00±3.07	91.30±3.78	47.22±2.69	97.00±3.88	Reversible
TC9	89.00±4.22	96.03±3.77	44.03±3.01	91.60±5.55	Reversible
TC10	79.88±3.46	94.01±2.56	58.00±4.05	93.22±2.30	Reversible
TC11	85.00±3.49	91.90±4.00	57.22±2.90	90.33±3.87	Reversible

*hMAO isoforms were preincubated with no inhibitor, with the newly synthesized compounds and also with the reference inhibitors (at concentrations equal to fivefold of their IC₅₀ values for the inhibition of hMAO-A and – B) for 15 min, and enzyme activities were measured. The mixtures were then dialyzed for 24 h and residual activities were determined. Each value represents the mean±SEM of three independent experiments.

Table 3: *In vitro* cytotoxicity of the TC series in HepG2 cells.

Compounds	Viability (%)		
	1 μ M	10 μ M	100 μ M
1	94.84 \pm 1.82	90.61 \pm 1.29	88.31 \pm 4.63
2	93.01 \pm 1.62	85.68 \pm 4.96	86.04 \pm 3.76
3	96.12 \pm 2.01	88.54 \pm 1.40	89.63 \pm 0.99
4	90.77 \pm 2.11	89.42 \pm 2.61	84.57 \pm 3.59*
5	91.29 \pm 1.37	85.15 \pm 3.69*	79.17 \pm 5.32*
6	92.28 \pm 2.12	87.60 \pm 1.61	79.54 \pm 4.42*
7	91.13 \pm 2.07	85.50 \pm 3.28*	75.70 \pm 0.84**
8	91.55 \pm 1.41	87.24 \pm 2.49	80.98 \pm 4.25*
9	93.55 \pm 3.19	88.39 \pm 1.29	86.07 \pm 3.27
10	90.89 \pm 3.35	87.25 \pm 2.66	74.36 \pm 2.18**
11	90.30 \pm 0.57	85.51 \pm 3.17*	76.77 \pm 1.75**

Data were expressed as mean \pm SEM (n=3). Cell viability was expressed as a percentage of the control value. p<0.05 was considered as statistically significant.

(* P<0.05, ** P<0.01 vs control)

Table 4. Component energy of the docked compounds with hMAO-isoforms from AutoDock 4.2

Enzyme	Compound code	EE	VdW	TFE
hMAO-A (PDB: 2BXR)	TC1	-0.11	-8.63	+1.19
	TC2	-0.22	-8.59	+1.49
	TC3	-0.08	-9.06	+1.49
	TC4	-0.11	-8.77	+1.19
	TC5	-0.15	-9.32	+1.49
	TC6	-0.15	-9.72	+1.49
	TC7	-1.32	-8.72	+1.49
	TC8	-0.20	-9.07	+1.19
	TC9	-0.04	-9.19	+1.19
	TC10	-0.14	-8.57	+1.19
	TC11	-0.18	-8.81	+1.49
hMAO-B (PDB: 2BYB)	TC1	-0.01	-9.05	+1.19
	TC2	-0.07	-9.44	+1.49
	TC3	-0.06	-9.92	+1.49
	TC4	+0.02	-9.31	+1.19
	TC5	-0.01	-10.03	+1.49
	TC6	-0.02	-10.44	+1.19
	TC7	+0.17	-9.46	+1.49
	TC8	-0.02	-9.66	+1.19
	TC9	-0.02	-9.89	+1.19
	TC10	-0.02	-8.99	+1.19
	TC11	+0.01	-9.32	+1.49

EE: Electrostatic energy; Vdw: Vander Wal energy; TFE: Torsional Free energy

Table 5: The binding free energy of compound TC6 with MAO-A and MAO-B using the results from both MM-GBSA and MM-PBSA methods

GBSA		TC6-MAO-A						
		ΔE_{vdw}	ΔE_{elec}	ΔE_{EGB}	ΔE_{ESURF}	ΔG_{gas}	ΔG_{solv}	ΔG_{bind}
TC6-MAO-A	Normal	-42.075 ± 0.070	-7.396 ± 0.077	17.517 ± 0.044	-5.291 ± 0.006	-49.471 ± 0.099	12.226 ± 0.044	-37.245 ± 0.084
	AMD	-39.946 ± 0.074	-6.338 ± 0.106	16.338 ± 0.050	-5.104 ± 0.006	-46.284 ± 0.144	11.234 ± 0.048	-35.050 ± 0.122
TC6-MAO-B	Normal	-42.199 ± 0.067	-18.208 ± 0.099	23.044 ± 0.080	-5.350 ± 0.004	-60.407 ± 0.103	17.693 ± 0.080	-42.714 ± 0.104
	AMD	-43.192 ± 0.065	-10.624 ± 0.103	22.530 ± 0.091	-5.387 ± 0.004	-53.816 ± 0.100	17.143 ± 0.091	-36.674 ± 0.072
PBSA								
		ΔE_{vdw}	ΔE_{elec}	ΔE_{EPB}	$\Delta E_{ENPOLAR}$	ΔG_{gas}	ΔG_{solv}	ΔG_{bind}
TC6:MAO-A	Normal	-42.075 ± 0.070	-7.396 ± 0.077	31.143 ± 0.084	-3.655 ± 0.003	-49.471 ± 0.099	27.488 ± 0.083	-21.983 ± 0.114
	AMD	-39.946 ± 0.074	-6.338 ± 0.106	28.742 ± 0.086	-3.652 ± 0.003	-46.284 ± 0.144	25.090 ± 0.085	-21.194 ± 0.146
TC6-MAO-B	Normal	-42.199 ± 0.067	-18.208 ± 0.099	38.607 ± 0.108	-3.648 ± 0.003	-60.407 ± 0.103	34.958 ± 0.108	-25.448 ± 0.122
	AMD	-43.192 ± 0.065	-10.624 ± 0.103	37.410 ± 0.122	-3.750 ± 0.003	-53.816 ± 0.100	33.660 ± 0.123	-20.157 ± 0.101

Table	Normal	Values \pm error	AMD	Values \pm error	6: Decomposition analysis showing the residues that have the energy changes during MD and AMD of the receptor interaction the result from only GBSA
top ten highest the ligand-using MM-	POS 1	-20.119 \pm 1.414	POS 1	-18.654 \pm 1.921	
	ASN 166	-2.515 \pm 1.352	TYR 426	-1.872 \pm 0.424	
	ILE 165	-1.913 \pm 0.413	PHE 193	-1.810 \pm 0.406	
	TYR 389	-1.820 \pm 0.363	ASN 166	-1.716 \pm 0.911	
	PHE 193	-1.694 \pm 0.384	TYR 389	-1.672 \pm 0.347	
	TYR 426	-1.502 \pm 0.457	ILE 165	-1.543 \pm 0.398	
	ILE 317	-1.060 \pm 0.443	ILE 317	-1.315 \pm 0.296	
	ILE 192	-1.047 \pm 0.469	ILE 192	-1.312 \pm 0.477	
	PHE 162	-0.711 \pm 0.396	ILE 307	-0.784 \pm 0.361	
	ILE 307	-0.662 \pm 0.385	PHE 162	-0.440 \pm 0.283	
TC6-MAOB					
	Normal	Values \pm error	AMD	Values \pm error	
	POS 1	-23.503 \pm 2.005	POS 1	-19.696 \pm 1.210	
	TYR 434	-2.515 \pm 0.469	TYR 397	-2.115 \pm 0.519	
	TYR 59	-2.227 \pm 0.548	TYR 434	-2.074 \pm 0.684	
	TYR 397	-1.848 \pm 0.379	LEU 170	-1.869 \pm 0.599	
	GLN 205	-1.404 \pm 0.512	GLN 205	-1.270 \pm 0.537	
	SER 58	-1.195 \pm 0.577	ILE 198	-1.145 \pm 0.711	
	GLY 57	-1.065 \pm 0.505	TYR 325	-0.863 \pm 0.378	
	MET 435	-0.927 \pm 0.282	TYR 59	-0.811 \pm 0.400	
	LEU 327	-0.924 \pm 0.327	PHE 167	-0.676 \pm 0.369	
	PHE 342	-0.900 \pm 0.238	PHE 342	-0.647 \pm 0.246	